D2.5 - WP2 lab: testing of methods and tools

D2.5 WP2 lab: testing of methods and tools

Summary

Deliverable 2.5 of project ICARIA is the main outcome of Task 2.4 (WP2 lab: testing of methods and tools). This task focuses on developing and testing those designed to assess different climate hazards and related issues, such as the joint probability of compound events. The emphasis is on new methods and tools for which the consortium does not have a strong background, such as compound hazard assessment. The aim is to ensure that these methods and tools are robust and ready for implementation in WP4. This testing phase is crucial for validating the effectiveness and reliability of the new approaches to identify potential gaps and barriers in advance and resolve them for the implementation of Trials and Minitrials before their future applications.

Deliverable number	Work package	
D2.5	WP2	
Deliverable lead beneficiary	**Deliverable author(s)**	**Contributor(s)**
IREC	Albert Gili (IREC) Àlex de la Cruz (AQUATEC) Lucia Bohajar (AQUATEC) Júlia del Pozo (AQUATEC) Agustín Torres (AQUATEC) Marianne Bügelmayer-Blaschek (AIT) Nadia Politi (DMKTS) Barry Evans (UNEXE)	Elena Veza (AMB) Albert Chen (UNEXE) Athanasios Sfetsos (DMKTS) Ioannis Zarikos (DMKTS)
Internal reviewer(s)	**External reviewer(s)**	
Barry Evans (Organization)	Beniamino Russo (UPC)	
Planned delivery date	**Actual delivery date**	
30/06/2024	28/06/2024	
Dissemination level	X PU = Public ☐ PP = Restricted to other programme participants ☐ RE = Restricted to a group specified by the consortium. Please specify: _____ ☐ CO = Confidential, only for members of the consortium	

Document history

Date	Version	Author	Comments
22/03/2024	1.0	Albert Gili (IREC)	Included outline of document and presented to the contributors.
17/04/2024	2.0	Albert Gili (IREC)	Adapted to the same format as other lab tasks.
28/06/2024	3.0	All authors	Final versions by taking into account the review process.

Table of contents

List of Figures

List of Tables

List of Acronyms and Abbreviations

AMB	Barcelona Metropolitan Area
AOI	Area Of Interest
BUI	Buildup Index
CFFDRS	Canadian Forest Fire Danger Rating System
CI	Critical infrastructure
CLM	Climate Limited-area Modelling
CNIG	National Geographic Information Center
CS	Case study
DC	Drought Code
DMC	Duff Moisture Code
DSM	Digital Surface Model
DSS	Decision support system
EFFIS	European Forest Fire Information System
FFMC	Fine Fuel Moisture Code
FWI	Fire Weather Index
GEE	Google Earth Engine
GIS	Geographic Information System
HNMS	Hellenic National Meteorological Service
HW	Heat Waves
ISI	Initial Spread Index
LST	Land Surface Temperature
MT	Meteorological Tide
NDVI	Normalised Difference Vegetation Index
NIR	Near Infrared

PET	Physiological Equivalent Temperature
RAF	Resilience Assessment Framework
RP	Return Periods
S	Wave Setup
SAR	South Aegean Region
SIOSE	Information System on Land Occupation in Spain
SLZ	Salzburg Region
SOLWEIG	SOlar and LongWave Environmental Irradiance Geometry model
SPEI	Standarised Precipitation Evapotranspiration Index
SPI	Standardized Precipitation Index
SS	Storm Surge
SSO	Strategic Subobjectives
UHI	Urban Heat Island
UTCI	Universal Thermal Comfort Index
UTFVI	Urban Thermal Field Variation Index
WP	Work package
WRF	Weather Research & Forecasting Model

Executive summary

The present deliverable is the collection of the tests conducted in the Work Package 2 frame of the ICARIA project. Throughout the previous tasks, Work Package 2 is dedicated to modelling, analysing, and evaluating the likelihoods of different climate and weather-driven hazards, their interactions as the triggering, and the consequences of combined or compound hazards.

Therefore, the objective of the deliverable is to create and conduct simulations to test new or not consolidated methods and tools for hazard assessment developed in the previous tasks of the same work package. The selection of the tests takes into account the three regions under study of the project as well as the selected hazards that affect them. These are assigned where the consortium does not have a strong background in order to detect possible barriers or gaps and to minimise them for implementation in the Trials and Minitrials.

The test carried out in this task are:

    A.   Application of the Heat Wave hazard model to the Barcelona Metropolitan Area case study

    B.   Application of the Extreme wind hazard model to the Salzburg Region case study

    C.   Application of the Drought hazard model to the South Aegean Region case study

    D.   Evaluation of the joint probability of occurrence of multi-hazard events for the Trial scenarios of the three case studies

    E.   Integration of Heat Wave hazard with the impact models on the electricity sector

    F.   Implementation of compound event hazard, Wildfire and Drought, to the South Aegean Region case study

The first three tests (A, B, and C) analyse single hazard models. The results of test A get, throughout the Heat Wave maps and applying the SOLWEIG model, the Urban Heat Island temperatures and the recognition of the hot and cold spots of the region. Test B analyses the scarcity of the observational wind gust data, which may lead to high uncertainties for the extreme wind hazard models. Test C bases the classification of the Drought periods on the SPI variable and gives the frequency distribution for the historical and future scenarios. Test D is focused on the joint probability distribution of occurrence of multiple hazards consecutively and simultaneously, providing the return period of happening for several multiple hazards and their case study region. In another case, Test E analyses the interaction of the hazard with the electric sector and computes its possible impacts. Test F results are the statistical analysis of the events under study (Wildfire and Drought) occurring simultaneously by checking if the indicators of both hazards exceed the threshold.

1   Introduction to project ICARIA

The number of climate-related disasters has been progressively increasing in the last two decades and this trend could be drastically exacerbated in the medium- and long-term horizons according to climate change projections. It is estimated that, between 2000 and 2019, 7,348 natural hazard-related disasters have occurred worldwide, causing 2.97 trillion US$ losses and affecting 4 billion people (UNDRR, 2020). These numbers represent a sharp increase of the number of recorded disaster events in comparison with the previous twenty years. Much of this increase is due to a significant rise in the number of climate-related disasters (heatwaves, droughts, flooding, etc.), including compound events, whose frequency is dramatically increasing because of the effects of climate change and the related global warming. In the future, by mid-century, the world stands to lose around 10% of total economic value from climate change if temperature increase stays on the current trajectory, and both the Paris Agreement and 2050 net-zero emissions targets are not met.

In this framework, **Project ICARIA** has the overall objective to promote the definition and the use of a comprehensive asset level modeling framework to achieve a better understanding about climate related impacts produced by complex, compound and cascading disasters and the possible risk reduction provided by suitable, sustainable and cost-effective adaptation solutions.

This project will be especially devoted to critical assets and infrastructures that are susceptible to climate change, in a sense that its local effects can result in significant increases in cost of potential losses for unplanned outages and failures, as well as maintenance – unless an effort is undertaken in making these assets more resilient. ICARIA aims to understand how future climate might affect life-cycle costs of these assets in the coming decades and to ensure that, where possible, investments in terms of adaptation measures are made up front to face these changes.

To achieve this aim, ICARIA has identified 7 Strategic Subobjectives (SSO), each one related to one or several work packages. They have been classified according to different categories: scientific, corresponding to research activities for advances beyond the state of the art (SSO1, SSO2, SSO3, SSO4, SO5); technological, suggesting and/or developing novel solutions, integrating state-of-the art and digital advances (SSO6); societal, contributing to improved dialogue, awareness, cooperation and community engagement as highlighted by the European Climate Pact (SSO7); and related to dissemination and exploitation, aimed at sharing ICARIA results to a broader audience and number of regions and communities to maximise project impact (SSO7).

- SSO1.- Achievement of a comprehensive methodology to assess climate related risk produced by complex, cascading and compound disasters

- SSO2.- Obtaining tailored scenarios for the case studies regions

- SSO3.- Quantify uncertainty and manage data gaps through model input requirements and innovative methods

- SSO4.- Increase the knowledge on climate related disasters (including interactions between compound events and cascading effects) by developing and implementing advanced modeling for multi-hazard assessment

- SSO5.- Better assessment of holistic resilience and climate-related impacts for current and future scenarios

- SSO6.- Better decision taking for cost-efficient adaptation solutions by developing a Decision Support System (DSS) to compare adaptation solutions

- SSO7.- Ensure the use and impact of the ICARIA outputs

2 Objectives and context of the deliverable

Work Package 2 (WP2), entitled "Multi-hazard modelling and assessment," focuses on the methodologies and tools used to model multi-hazard scenarios. Figure 1 shows the variety of hazards, risk receptors, and cascading effects considered in the three regions studied.
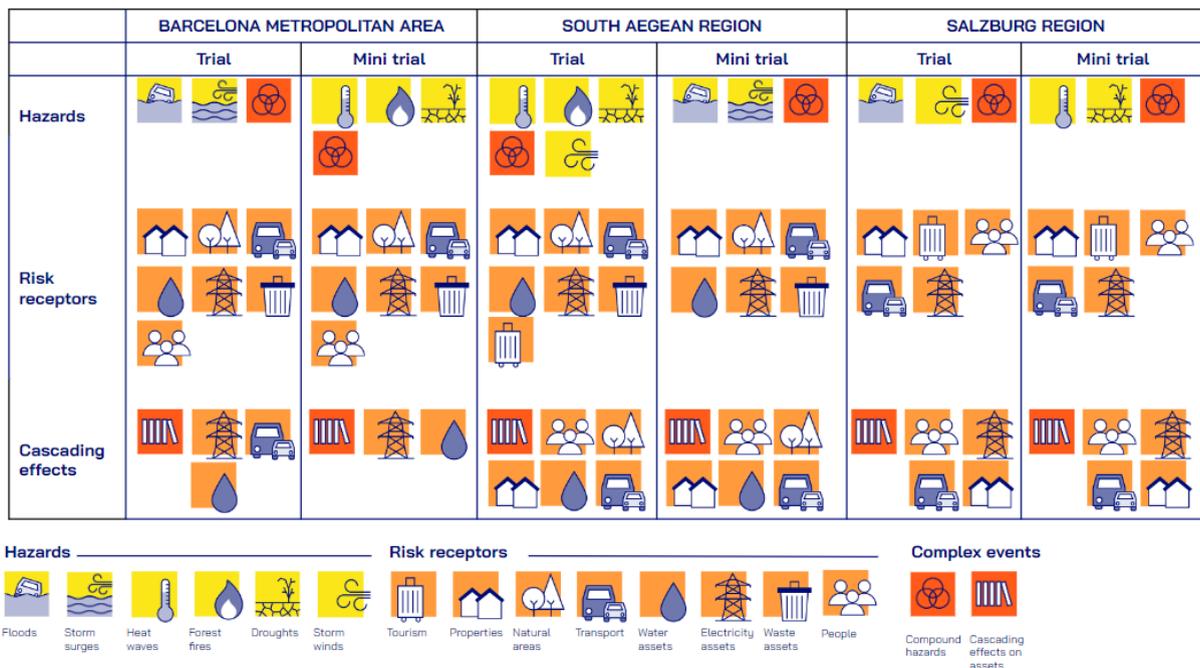
Figure 1. Summary of hazards and risk receptors considered in the different CS of ICARIA.

This deliverable, D2.5 "WP2 lab: testing of methods and tools," contains the developments and results of task 2.4, which is the last task in WP2 and tests the methods and tools developed in WP2. The previous tasks in WP2 consisted of outlining the conceptual and methodological basis for hazard risk assessment (D2.1), detailing mathematical approaches and models for quantifying the joint probabilities of compound multi-hazard events (D2.2), and defining an adaptable framework for simulating various compound hazard events (D2.3). These deliverables included descriptions of main hazards, analyses of their interactions, examples of recent extreme events, types of compound events to be modelled, and guidelines for selecting input parameters and coupling tools for multi-hazard assessment.

Therefore, D2.5 aims to test the outcomes of the previous hazard for ease of their implementation in both trials and mini-trials by identifying potential barriers or gaps in advance. Strategies and countermeasures are devised to address these identified challenges and setbacks effectively. The implementation process is facilitated by providing guidance and support to project stakeholders. Additionally, recommendations are suggested to enhance the replicability of the case study or other related studies in subsequent work packages. Finally, improvements and refinements to tested methodologies are advised for ongoing enhancement and optimization.

In order to do it, six specific tests are proposed for execution in this task to achieve its objectives. The aim of all tests is to encompass all dimensions of the work conducted within WP2 across the three case studies. Consequently, each Case Study (CS) is represented in at least two tests. Additionally, the three preliminary tasks of the work package are also implemented. Table 1 serves as a compilation of all items subjected to testing.

Table 1. List of tests conducted in the task.

Test	Issue	CS	Partners involved
A	Application of the Heat Wave hazard model to the AMB CS	AMB	AQUA, AMB
B	Application of the Extreme wind hazard model to the SLZ CS	SLZ	AIT
C	Application of the Drought hazard model to the SAR CS	SAR	DMKTS
D	Evaluation of the joint probability of occurrence of multi-hazard events for the Trial scenarios of the 3 CS	3 CS	UNEXE + 3CS
E	Integration of hazard models with the impact models on the electricity sector	AMB	IREC, AQUA, AMB
F	Assess compound hazards event (Wildfire + Drought) to the SAR CS	SAR	DMKTS

The deliverable conducts the majority of the tests separately for two reasons. Firstly, to allow each contributor to focus specifically on a particular task in order to identify its challenges and detail possible improvements, as mentioned previously. Secondly, this approach facilitates parallel testing. The short timeframe of the deliverable makes it challenging to generate tests where one depends on another.

3 Methodology followed

The methodology employed for each of the six tests conducted in Task 2.5 follows a systematic and structured approach. It begins with a clear delineation of the test's objectives and boundaries, followed by the implementation of the designated hazard model or tool within the specified case study region. Subsequently, the obtained results adequacy and alignment with the project needs are assessed. Any discrepancies or errors encountered during the process are meticulously identified, and considered to propose enhancements or modifications to improve the applicability of the tested developments. Figure 2 depicts this process.

Scope definition → Model/tool implementation → Results adequacy assessment → Gaps and errors identification → Define possible improvements

Figure 2. Scheme of the test development in Task 2.5.

Activities done in each step of the test are as follows:

1. **Scope definition**

   Definition of the objectives and scope of each test. Specifying the hazard model or tool being implemented, the case study region involved and the desired outcomes.

2. **Model/tool implementation**

   Actual implementation of the chosen hazard model or tool within the designated case study region. This involves setting up the necessary parameters, running simulations and/or performing assessments and generating relevant data.

3. **Results adequacy assessment**

   Evaluation of the adequacy of the results obtained from the implementation phase. Assess whether the outcomes align with the predefined objectives and if they provide meaningful insights into the resilience and risk factors considered.

4. **Gaps and errors identification**

   Identify any shortcomings, gaps or errors encountered during the implementation or assessment stages. This may include discrepancies between expected and actual results, limitations in data availability or quality, or technical issues with the models or tools used.

5. **Possible improvements definition**

   Propose potential enhancements or modifications to be applied to the tested methods or tools to address the identified gaps and errors. This could involve refining parameters, updating algorithms, incorporating additional data sources, or improving the usability of the tools for stakeholders.

Section 4 presents the implementation of this testing methodologies to the cases presented in Table 1.

4 Test developed

4.1 Test A: Heat island hazard model to the AMB CS

4.1.1 Summary and objectives of Test A

The objective of Test A has been focussed on analysing the effect of rising temperatures and heat waves on the Urban Heat Island (UHI) phenomenon in the AMB. Based on these analyses and other relevant information about the territory and AMB population, the final objective is to create a model in selected critical or special interest areas.

To develop the Heat Island Hazard model in the AMB, the SOLWEIG model (Lindberg, 2008) has been selected. SOLWEIG is a radiation model that simulates the spatial variations of 3D radiation fluxes and Mean Radiant Temperature (Tmrt) in complex urban environments. The model requires a limited number of inputs, such as direct, diffuse and global shortwave radiation, air temperature, relative humidity, urban geometry and geographical information.

The large size of the AMB requires a very large computational effort to be able to apply a model such as SOLWEIG to its full extent. The amount of information that needs to be prepared and processed makes it unfeasible within the limits of the project. That is why first of all, as part of the test, a study has been carried out to analyse the state of the AMB territory in UHI terms, taking Land Surface Temperature (LST) as a reference parameter.

In order to prioritise and select areas of interest for the model application, a vulnerability index is implemented and, once the study area has been selected, the model is applied as the final phase of the test on one of them.

Table 2. Test A summary.

Test A summary			
Tested tool	Heat island model	**Test responsible**	AQUATEC
Developer of the tool	AQUATEC	**CS of the test**	AMB

4.1.2 Activities of Test A

To analyse UHI effect in the AMB and apply the Heat Island model, the following activities have been carried out:

- In first place, a preliminary study of the UHI phenomenon in the AMB and definition of the study months.
- Extension of the HW phenomenon and identification of peri-urban cold areas (MODIS night-time LST).

- Identification of urban areas with a higher impact of UHI. Climate and Landsat 8 analysis.
- Vulnerability index and critical areas selection. The vulnerability index based on different social and urban factors, will identify the most vulnerable areas to heat island effects. This index will be cross-referenced with the most affected areas by UHI.
- Finally a Climate modelling (Urban Heat Island Model) will be implemented in selected critical areas.

Remote sensing and climate analysis.

- **Preliminary analysis and critical period determination of the UHI phenomenon**.

  Dataset Used: *MODIS data set - MOD11A1.061 Terra, Land Surface Temperature (LST) and Emissivity Daily Global. 1km resolution*.

  This dataset provides daily data of night-time surface temperature (LST_Night_1km band) with a 1000m resolution. Three years have been selected with a 10-year interval starting from the last complete year (2023, 2013 and 2003) to carry out a temporal analysis of the annual night-time LST, and identify the highest surface temperatures in order to define the critical periods (summer months) susceptible of being affected by UHI. In addition, these results have been processed with a Geographical Information System (GIS) to cross reference them with land use information from SIOSE (Information System on Land Occupation in Spain, integrated into the National Territory Observation Plan) and finally, to establish the spatial extension of the UHI (hot areas/urban zones) and location and distribution of the cold areas that will serve as a reference for subsequent calculations.

- **Critical area identification: UHI and Heat Waves.**

  Dataset Used: *Landsat 8 dataset USGS Landsat 8 Level 2, Collection 2, Tier 1 (Thermal band resolution: 30m, revisit period: about one every two weeks)*.

  The effect of the UHI phenomenon is enhanced during Heat Waves (HW) (Ward, et al., 2016; He, et al., 2020; Posegga, et al., 2020; Zhao, et al.,2018). In order to identify the years with the highest number of heat waves and the greatest amplitude (number of days), a study has been carried out, considering the AEMET (Agencia Estatal de Meteorología) definition of HW and using the daily maximum temperature data collected from the official stations distributed in the AMB.

  The Landsat 8 dataset has been used for a more accurate analysis of the day LST in urban territory, under the methodology for calculating LST, UHI index (Normalised Urban Heat Island Index) and UTFVI (Urban Thermal Field Variation Index) established by Waleed et al. (2021) for Google Earth Engine (GEE). In this case, a mask for clouds, cloud-generated shadows and pixel quality has been applied. After filtering and selection of images for each period, the LST has been calculated by selecting the band 'ST_B10', based on these data, the UTFVI and UHI have been also calculated. UTFVI is used for the evaluation of the UHI effect considering the ecological aspects of the city (Renard, F. et al., 2019). The calculation formula is as follows:

$$UTFVI \ = \ LST \ - \ LSTmean(aoi)/LST \quad (Eq. \ 1)$$

where LST is the temperature associated with the pixel and LSTmean(aoi) is the average temperature of the area of interest. The UHI, Normalised Urban Heat Island Index:

$$UHI \ = \ (LST \ - \ LSTmean(aoi))/stdLST \quad (Eq. \ 2)$$

where LST is the Land Surface Temperature of the pixel, LSTmean(aoi) the mean LST of the study area and stdLST the standard deviation of the LST of the pixel. These operations apply for selected years, calculating it for the whole year, the summer period and HW period with the highest number of days.

- **Green areas identification (Climate shelters).** Green areas in urban planning play a major role in climate change mitigation. They are considered climate shelters providing thermal comfort to the population in extreme temperature events and having a temperature-reducing effect in the surroundings. External climate shelters are green spaces with a surface area > 0.5 ha and an Normalised Difference Vegetation Index (NDVI) > 0.4, based on the definition of the Barcelona Climate Shelter Network (Ajuntament de Barcelona, 2019). The NDVI is an index of photosynthetically active biomass. The calculation formula is:

$$NDVI \ = \ (NIR \ - \ Red) \ / \ (NIR \ + \ Red) \quad (Eq. \ 3)$$

where NIR is the Near Infrared band (B8) and Red is the red band (B4). The surface considered has an NDVI value >0.4 and crossed with the SIOSE land use layer reclassified on the land uses that will be applied in SOLWEIG model (paved, buildings, evergreen trees, deciduous trees, Grass surfaces, bare soil and water) to establish the spatial extent of green areas.

Vulnerability index and critical area selection

The social, economic and habitability conditions of under-resourced people increase the risks and makes them even more vulnerable to the rise in urban temperatures, with excessive heat leading to increased mortality and morbidity. In order to identify and map the population particularly vulnerable to high temperatures, a vulnerability index has been developed. The methodology implemented is based on different parameters disaggregated into census sections, which are classified according to the risk magnitude. These parameters are:

- **Social**: (i) People under 16 years old; (ii) People over 65 years old, (iii) Population density, (iv) Average gross income per household. Data source: Instituto de Estadística de Cataluña (IDESCAT).
- **Households**: (i) Year of construction; (ii) Energy efficiency. Data source: URBAN3R, Open Data Platform to promote urban regeneration in Spain (Ministerio de Transporte, Movilidad y Agenda Urbana, 2023).
- **Urban**: (i) Existing green areas smaller than 0,5 ha. Data source: Sistema de Información sobre Ocupación del Suelo de España (SIOSE).

After identifying these vulnerable areas, the information is crossed with the high temperature zones analysed by remote sensing described above. The result of this analysis gives us the critical areas

that have a greater exposure to high temperature risks, which are the object of analysis for the climate model.

Climate modelling: Urban Heat Island Model

For the development of microclimatic studies on the impact of solar radiation and temperature on environmental health in the identified critical areas of the AMB, the **SOLWEIG model (SOlar and LongWave Environmental Irradiance Geometry model)** has been implemented.

SOLWEIG is a model which can be used to estimate spatial variations of 3D radiation fluxes and mean radiant temperature (Tmrt) in complex urban settings. The SOLWEIG model follows the same approach commonly adopted to observe Tmrt (as used by Höppe (1992)), with shortwave and longwave radiation fluxes from six directions being individually calculated to derive Tmrt. The model requires a limited number of inputs, such as direct, diffuse and global shortwave radiation, air temperature, relative humidity, urban geometry and geographical information (latitude, longitude and elevation). Additional vegetation and ground cover information can also be used to improve the estimation of Tmrt. Figure 3 outlines a flowchart of the SOLWEIG model.
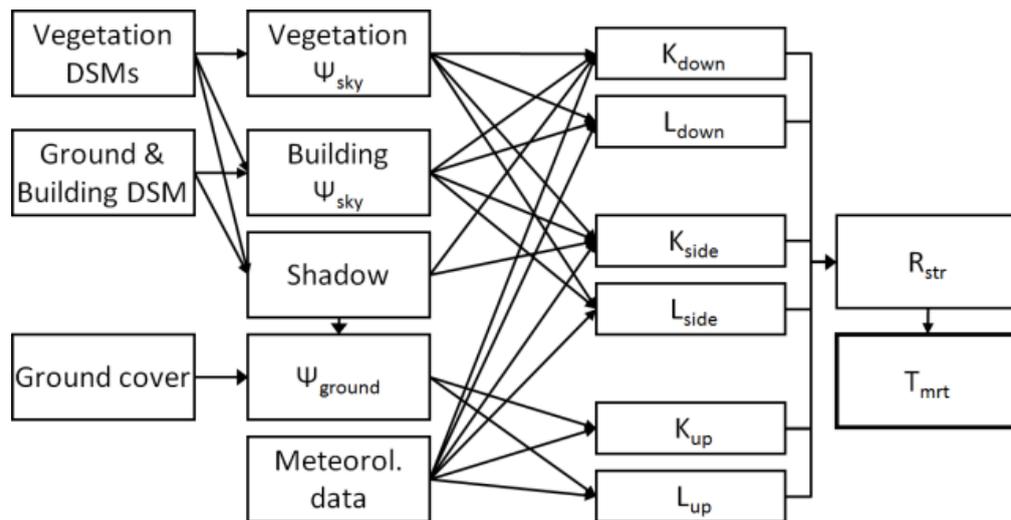
Figure 3. Flowchart of SOLWEIG model applied.

There are two categories of data needed to run SOLWEIG. The first category is the spatial information, outlined in Table 3. The second is meteorological data and other settings such as environmental and human exposure parameters.

Table 3. Spatial data needed and processed to run SOLWEIG, data correction required and identified challenges so far.

Spatial data	Description	Data source	Data correction required	Challenges
Building and Ground Digital Surface Model (DSM)	A DSM consisting of ground and building heights. This dataset also determines the latitude and longitude used for the calculation of Sun position. Shape cover.	National cadastre. National Geographic Information Center (CNIG).	To integrate the heights of the buildings, the number of storeys of each building has been multiplied by 3m. The heights obtained are corrected with LIDAR processed information.	It has been detected that the cadastre coverages have some errors that will have to be corrected manually for each critical area studied. Higher resolution DSMs should be employed to improve analysis.
Vegetation Canopy DSM	A DSM consisting of pixels with vegetation heights above ground.	LIDAR mapping database processed with vegetation identification (CNIG).	The data have been classified from heights of 3 metres to identify trees and exclude other vegetal cover. For this coverage it is parameterised by including other variables: Transmissivity of Light Through Vegetation (3%) or Percent of Canopy Height (25%), which can acquire default values.	Contains classification errors that need to be corrected. Look for alternative sources of vegetation for digitisation, e.g. tree inventories with height, canopy size, etc.
Land use cover scheme	Land cover grid with different kinds of uses and their environmental parameterization such as albedo and emissivity of ground.	Information System on Land Occupation in Spain (SIOSE)	Reclassification of land use classes to those required in SOLWEIG.	Reclassification of land uses with higher spatial resolution (it is recommended to use the SIOSE data source by performing a reclassification of the types as required in SOLWEIG).

Mandatory requirement relating to meteorological data is that it needs to be a continuous file or specific momentary values, which allows for the selection of long complete periods or periods related to extreme episodes of heat waves.

The variables required for SOLWEIG are air temperature (degC), relative humidity (%) and incoming shortwave radiation (W m-2). To calculate the Physiological Equivalent Temperature (PET) and Universal Thermal Comfort Index (UTCI), wind speed data is required.

In the implementation of the model, the EPW files available from the El Prat - Barcelona Meteorological Station have been used. This data source requires specific treatment to update the data to the last years of the study period and the identification of hot hours.

The analysis of climate scenarios will be implemented on this meteorological information dataset.

The SOLWEIG model allows studying thermal stress in the city and its influence on human health, by calculating indices such as PET and UTCI. These indices will allow to evaluate the risks derived from heat waves on human health.

4.1.3   Results of Test A

Remote sensing and climate analysis.

To have a broad time perspective, three years have been taken as reference, with an interval of 10 years between these. An analysis of the variation of the territorial average of nighttime LST during the year is carried out to identify the study period, in which the heat island phenomenon is most intense (Figure 4.).
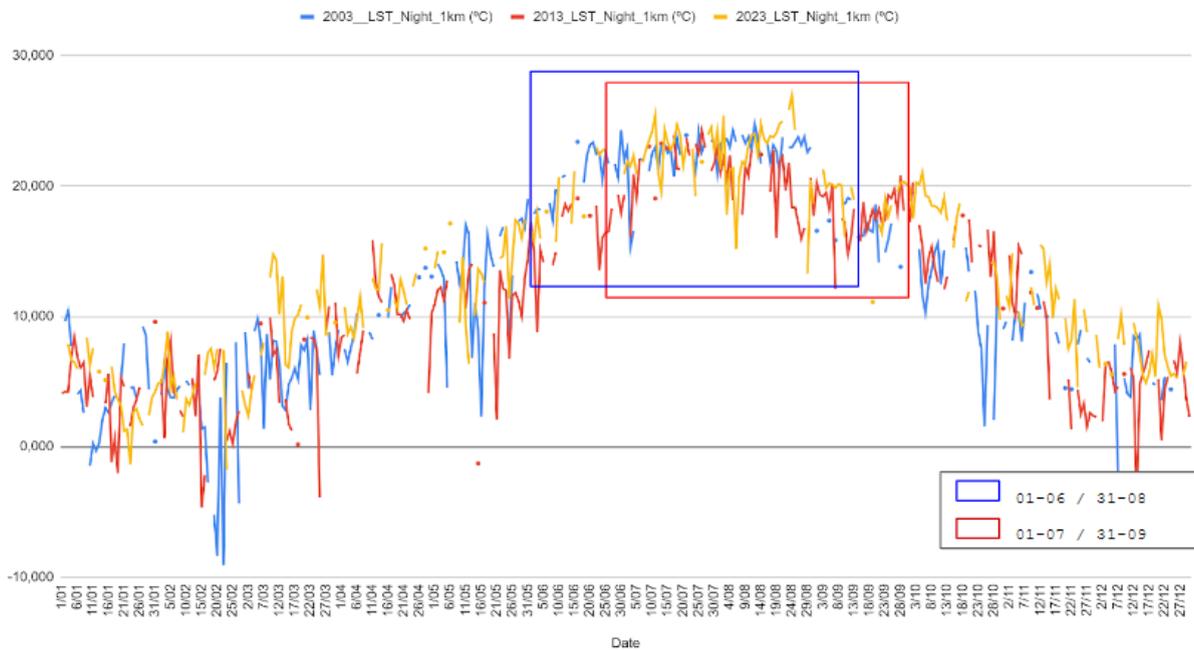
Figure 4. Daily average of Modis night-time LST for 2003, 2013 and 2023. Options evaluated for critical period selection: Blue mark June-Agost, red mark: July-September).

Figure 5 shows the annual average Modis nighttime LST for three selected years: 2003, 2013 and 2023.

LST máx = 16.196   LST máx = 14.922   LST máx = 16.359
LST min = 10.896   LST min = 9.568   LST min = 11.335
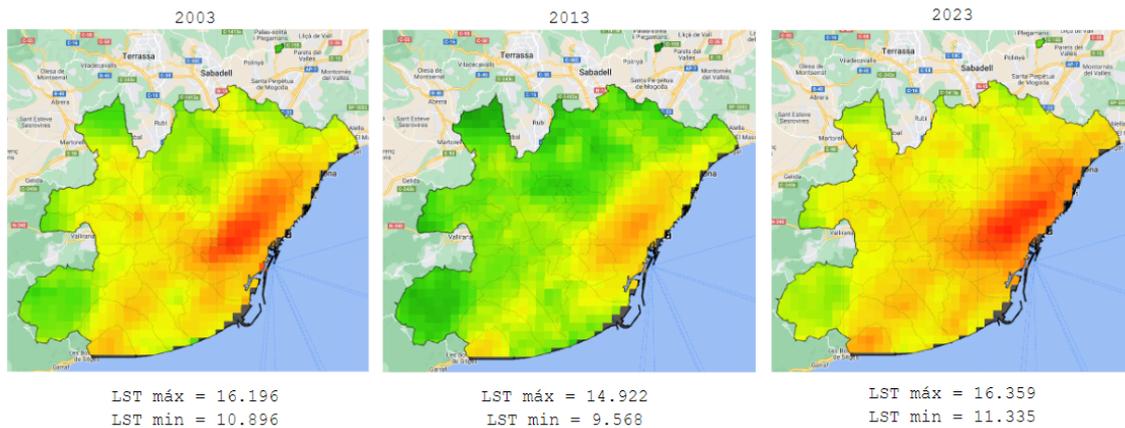
Figure 5. Spatial distribution of annual LST night-time average in 2003, 2013 and 2023.

Furthermore, these analyses have been used to delimit the HW extension, identifying periurban cold areas (Figure 6).
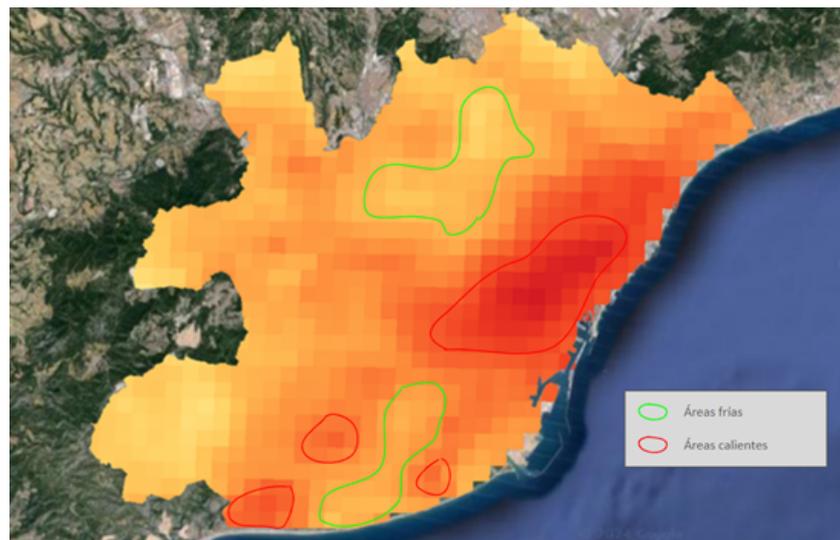
Figure 6. Hot and cool areas identification. 2023 Summer average of Modis night-time LST 1000m.

As a result of the climate analysis, the years with the highest number of heatwaves (HW) and longest duration were selected to perform this part of the test. It allows studying LST behaviour during heat waves. In order to carry out a more accurate analysis with higher spatial resolution of daytime LST in urban territory, UTFI and UH index are calculated using Landsat dataset. These indexes are calculated for the whole 3 years chosen, summer period and the largest HW period for each year. Table 4 summarises the main results extracted from the LST analysis to different time scales shown in Figure 7.

Table 4. Main results of daytime LST analisis to different time scales (year, summer (sum) and largest heat wave period (HW)) performed for 2018, 2019, 2022 and 2023.

Time period	2018			2019			2022			2023		
	year	sum	hw	year	sum	hw	year	sum	hw	year	sum	hw
Start date	01-01	01-06	30-07	01-01	01-06	26-06	01-01	01-06	28-07	01-01	01-06	20-08
End date	31–12 (+1)	31-08 (+1)	09-08 (+1)	31-12 (+1)	31-08 (+1)	30-06 (+1)	31-12 (+1)	31-08 (+1)	14-08 (+1)	31-12 (+1)	31-08 (+1)	25-08 (+1)
Heat wave length	-	-	11	-	-	5	-	-	18	-	-	5
Mean LST AMB	26.70	41.48	46.53	27.61	40.62	43.87	30.63	44.51	43.98	30.57	41.84	42.84
Std LST AMB	4.10	4.70	4.82	3.52	4.12	3.92	3.29	4.25	4.42	3.84	4.46	3.56
Min LST AMB	15.12	28.03	9.86	18.49	27.22	25.14	19.07	29.32	28.81	19.29	28.47	30.11
Máx LST AMB	36.23	50.49	58.13	35.53	49.84	52.31	39.1	56.29	55.03	38.10	49.21	49.22
Mean LST Coolest urban areas during nighttime	27.75	44.61	47.89	29.59	41.51	45.72	32.17	46.78	46.16	33.00	43.99	45.23
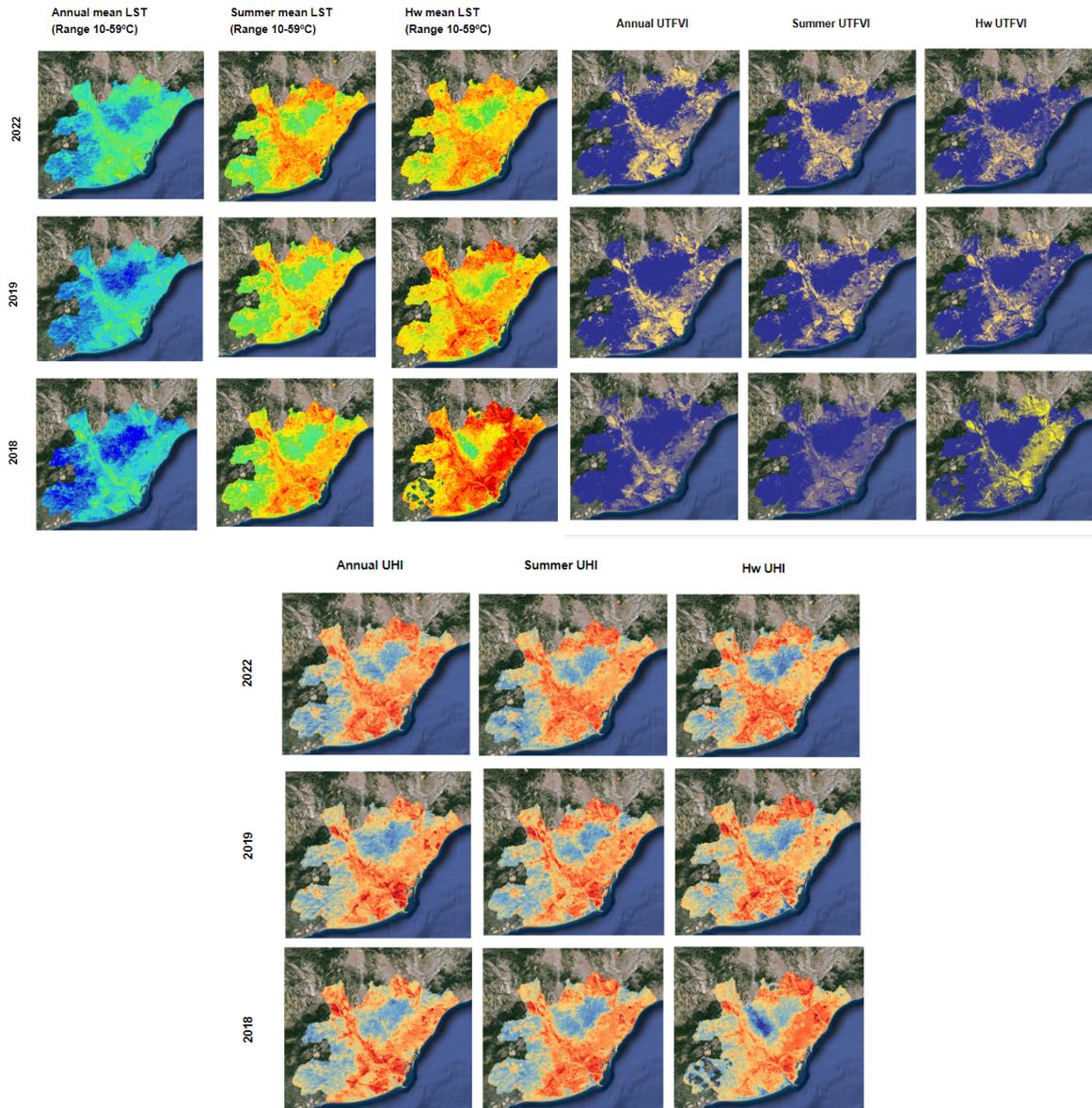
Figure 7. Landsat 8 LST average, UTFVI and UHI normalised index. Selected dates: Critical heat waves periods since 2013, summer period and year. Image collection USGS Landsat 8 Level 2, Collection 2, Tier 1 data set (about 10 am). Spatial resolution for thermal bands: 30m.

Vulnerability index and critical area selection

A vulnerability index is created with social, economic and urban data, which allows us to identify urban areas with high vulnerability to high temperature risks derived from the UHI. By putting together these results with the mean Landsat 8 LST explained above, it is possible to do a first approach to the selection of critical areas (areas with greater exposure to risks from high temperature), which are used for the climatic model.

Figure 8 shows the mean summer Landsat 8 LST in 2023 disaggregated into census sections (and a list of the municipalities with the highest LST) and an example of a first approach to the selection of a critical area.
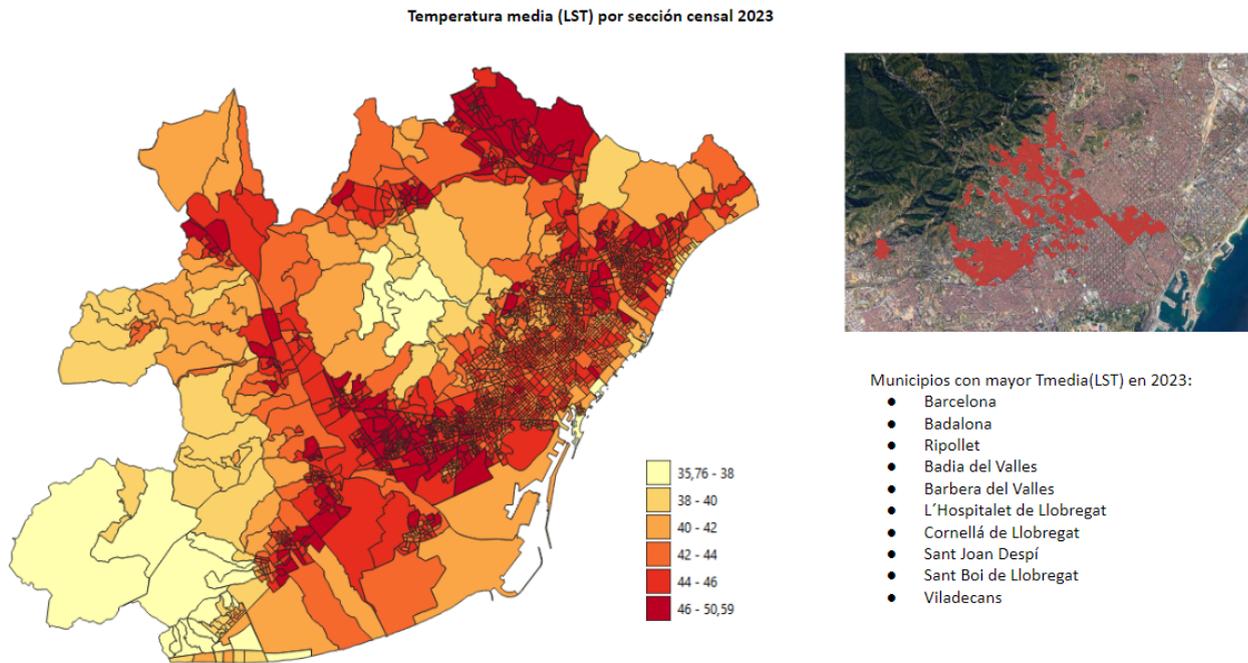
Figure 8. Mean summer Landsat 8 LST disaggregated into census sections in 2023 and an example of critical areas.

Climate modelling: Urban Heat Island Model

Figure 9 shows an example of implementing the SOLWEIG model in a critical area. This example has been carried out in Sants Station (Estación de Sants).
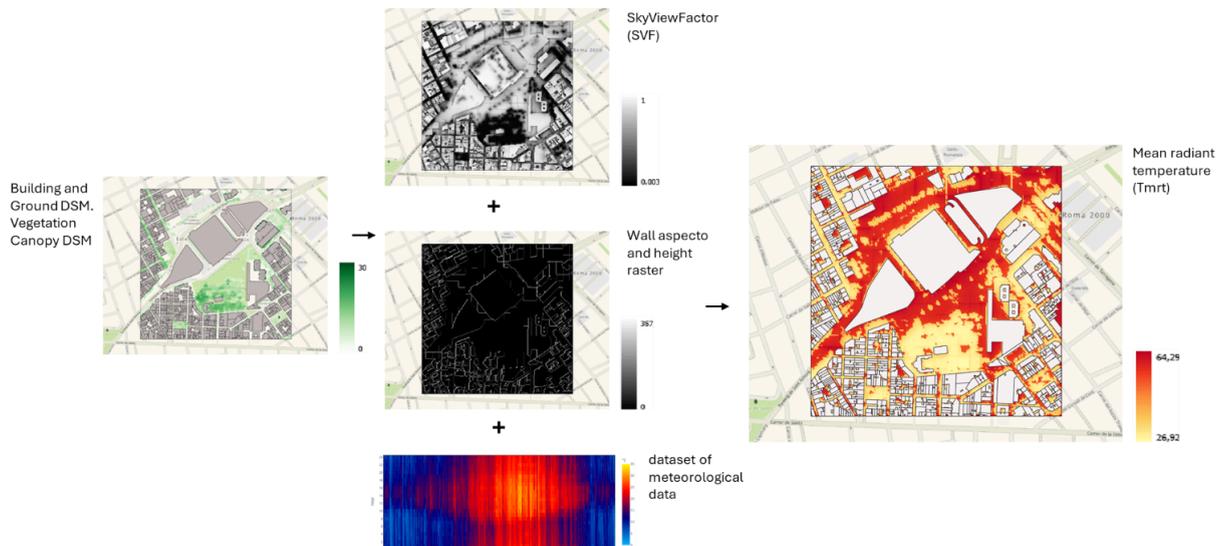
Figure 9. Simplified process of implementing the SOLWEIG model in a critical area of the city of Barcelona (Estación de Sants).

This test has provided a better understanding of climate impacts on heat island effect on AMB, the influence of heat waves on LST in urban areas and how the population may be affected across the territory. The test allowed a first approximation to be made in order to define the most critical areas within the AMB, identifying most affected spots and the most vulnerable population. Finally a practical example of SOLWEIGH model application has been carried out in one of these areas.

Some barriers were faced in carrying out this test. According to the definition of UHI, it is necessary to evaluate night temperatures, when the cooling is greatest in rural areas and the temperature difference between urban centres and the surroundings is largest. Remote sensing images make it possible to analyse this effect on the territory without intensive sensor deployments. The impossibility of using high resolution night-time images has led to use Landsat satellite images, which are daytime images but with a sufficient resolution to assess with wider detail the impact in urban areas and analyses the variation in temperature between neighbourhoods, the effect of industrial parks, the river, green areas within the city, ect. Landsat datasets are frequently used in recent years (Febrian, 2024; Halder et al., 2022; Hidalgo, 2021; Rees et al., 2024; Yuan et al., 2023) and have become in a very effective tool to evaluate this phenomenon due to the availability of a large number of data in large periods of time.

Another obstacle faced has been the data search for the vulnerability analysis. It has been complex to find all the necessary data disaggregated by the same territorial unit and from the most current time period possible. Socioeconomic parameters for which there is data by census section in the AMB have been selected. Ideally, up-to-date information would be available, but the most recent data from official sources in common for these parameters are from 2021.

In terms of the application of the climate model, there have been identified several barriers for further work. These barriers are related to the input data, as detailed processing and treatment of the required information layers, as some errors have been identified (listed in table 3).

Regarding the climate data for the model, a specific climate file is required that includes, among others, radiation data with hourly definition, this aspect is still to be worked on and refined.

Finally, due to the large computational effort and the processing of large amounts of data for the application of the model, it is necessary to further refine the critical areas. The criteria of the administration and the managers of the AMB should be used to select the areas of greatest interest in the application of the modelling within the critical areas. It will make the project more meaningful.

4.2 Test B Extreme wind hazard model to the SLZ CS

4.2.1 Summary and objectives of Test B

The objective of Test B has been focused on a first analysis of wind hazard models to be applied for Salzburg, as wind storms present a challenge to the region with respect to:

- damage of the protective forest
- forestry
- impact of fallen trees on the electrical infrastructure
- impact of fallen trees on the effectiveness of the flooding protection.

Even though the hazard wind storm has been clearly identified within the 1st CoP meeting at Salzburg, correctly representing wind within climate models poses a challenge - especially when focusing on wind gusts rather than mean wind speed.

Climate model projections have been performed within ICARIA using two methods (statistical, and dynamical, see D1.2) to produce state of the art high resolution meteorological conditions with respect to wind projections. Both methodologies face different challenges:

- **statistical**: wind observations are only rarely available (e.g. 2 wind vs 44 temperature observations), thus limiting the information needed for statistical downscaling; the spatial resolution of global climate models (~100 km x 100 km) doesn't allow them to represent local features that impact wind speed (e.g. orography, roughness length) and therefore aren't suited for providing local wind gust information.
- **dynamical**: if not defined differently, the hourly output values correspond to instantaneous values and don't represent the maximum value that occurred within the last hour. If the maximum value is needed, either an additional output parameter is activated or different post-processing methods exist. Within ICARIA two different models have been used, with one providing the maximum wind gusts, whereas the other needed a special set-up, which was activated only for the climate projections, but not the historical runs.

Based on the challenges regarding wind hazard modelling, the objectives of the test are (i) to understand the barriers available as well as potential solutions, (ii) the analysis of past events to understand the importance of wind direction.

Table 5. Test B summary.

Test B summary			
Tested tool	Extreme wind hazard data	**Test responsible**	AIT
Developer of the tool	AIT, FIC	**CS of the test**	SLZ

4.2.2 Activities of Test B

Within this test, different aspects regarding wind hazards have been considered:

- First analysis of available data for improved understanding of capability to represent gusts
- Review on methodologies to improve wind gust predictions (focusing on dynamical model output)
- CoP meeting to clarify impact and characteristics of wind storms

4.2.3 Results of Test B

Analysis of available data for improved understanding of capability to represent gusts

Concerning the statistical downscaling, wind gusts have been computed as output parameter based on available observation stations. However, as wind measurements are not available at all stations and wind gusts are difficult to measure (sometimes are even replaced by maximum mean wind due to this factor), this added to the complexity of the situations producing severe winds coupled with the importance of local characteristics such as orography, results in the uncertainty being much higher than for instance temperature evolution and a good density of observations is thus desirable. Regarding this downscaling, it seems as if wind gusts will weaken for the future climate conditions compared to past observations. However, Salzburg is a topographic area which is only partly resolved by the global climate models used as input, and only 2 observations are available in this regard here for the statistical downscaling. Therefore, the reliability of this data set is questionable - not due to the methodology applied, but due to the available data that is needed for statistical downscaling.

Regarding the dynamical downscaling, wind gusts also pose a challenge. Within the Climate Limited-area Modelling (CLM), the maximum wind gusts occurring hourly are output for past and future periods, allowing the direct validation towards past events and analysis of future development. However, for the Weather Research & Forecasting Model (WRF) only the mean wind is available for past and future periods, due to a namelist setting error for the past period. Apart from not having the requested output parameter for both models for the whole time period, additional challenges are:

- Observation data for validation: the used CHELSA data set (Karger et al., 2022, 2017) doesn't provide the parameter wind or wind gusts, therefore, observations will be used (same as for statistical downscaling) and for the years 2011 - 2014 also the INCA data set (Haiden et al., 2011) will be used to compare to past simulations. INCA starts 2011 and the model simulations driven with ERA5 are performed until 2014.
- Impact of local features on wind gusts is very strong, thus the capability of the models (WRF, 5 x 5 km, CCLM 2x2km spatial resolution) depends on the correctly used static input data and the methodology to compute wind gusts within the models. Further, extreme wind gusts often occur in combination with convective precipitation events, which also pose challenges in modelling.

To address these challenges, an in-depth comparison of the available model output data for past as well as future periods will be done (i) concerning maximum wind speed events for the past - compared

to available observations and INCA data, (ii) maximum occurring wind speeds during different climate states and future periods

CoP meeting to clarify impact and characteristics of wind storms

Within the second CoP meeting in Salzburg, the representatives defined hazardous wind characteristics stating that wind speeds > 90 km/h cause light damage, >120 km/h medium damage and >150 km/h severe damage. Furthermore, regarding the impact on forests, the importance of wind direction was stated as the mountain valleys are impacted differently by the same wind speeds with slightly different wind directions.

This information is crucial but poses another challenge since wind direction close to the surface is strongly impacted by surface and local conditions which are difficult to capture within climate models.

Review on methodologies to improve wind gust predictions

Within Stucki et al. (2017) four different post-processing methods for dynamical model output to retrieve wind gusts based on mean wind was performed, indicating that different methodologies exist. Within this study, the parameterizations used within WRF and CLM were applied, as well as two additional ones: the so-called Brasseur wind gust parameterization which is physics based and one using a constant multiplication factor which is based on observations. All four wind gust parameterizations display comparable errors compared to wind gust observations, indicating that even a very simplified one (multiplication of constant factor) might be applicable in case the constant is well defined. As 10 min wind (gust) observations are available for the Salzburg region from 1992 onwards, a regression between mean wind and wind gusts could be obtained and used as a first attempt to retrieve the wind gusts from the modelled mean wind speed.

Further, a student of the BOKU university has defined a new methodology on how to best post-process climate model data to retrieve wind gusts. As there are tight links between AIT and the BOKU, discussions are ongoing to share this methodology with AIT and to apply it within ICARIA. Another approach will be based on the AI based model weighting, where the available clime projections will be combined for an improved representation of hazards.

4.3 Test C: Drought hazard model to the SAR CS

4.3.1 Summary and objectives of Test C

The objective of this test is focused on meteorological drought assessment through the quantification of the historical and projected drought hazard in the SAR region, based on the use of the Standardised Precipitation Index (SPI) and frequency distribution diagrams.

The analysis of drought hazard by using this index is suitable, as SPI has been used widely in various recent drought assessment related studies for evaluating climate change effects on agriculture, hydrology, water resources and ecosystems.

Table 6. Test C summary.

Test C summary			
Tested tool	Drought Hazard model	**Test responsible**	DMKTS
Developer of the tool	DMKTS	**CS of the test**	SAR

4.3.2 Activities of Test C

The application of this methodology included primarily the calculation of SPI for the historical and future period for selected locations, based on daily precipitation datasets. These climate dataset were derived from the climate projections within ICARIA, by the application of statistical downscaling method, described in (Blázquez et al. 2024). For the realisation of the test, outputs for specific locations of the study area (e.g. Naxos, Kos and Rhodes), were processed accordingly, found here: https://intercambio.ficlima.org/indexed/ICARIA/Climate_projections/SAR/

For this trial test, climate datasets from MRI-ESM2-0, MPI-ESM1-2-HR, and EC-EARTH3, CMIP6 models were analysed for the historical period (1980-2014) and for the future period up to 2050, for SSP245 and SSP585 scenarios.

The SPI is calculated by fitting a probability density function to a given frequency distribution of precipitation (Faye Cheikh et al. 2019) and then the probabilities are transformed into a normalised distribution with a mean equal to zero and a variance of one, developed by Mckee et al. (1993). The distribution function used for computing SPI was the 'Gamma' as the most widely used in literature and recommended. Moreover, the SPI-6 was selected for drought hazard modelling, as in semi-arid and arid regions (as the study area) could give unreliable estimation of drought index computed at shorter accumulation periods (Karavitis et al 2014). SPI calculated as follows in the equation:

$$SPI = \frac{X_i - X_j}{\sigma} \quad (Eq.\ 4)$$

where, x_i refers to the current precipitation in the examined period, x_j refers to the mean precipitation of the timeseries, and σ refers to the standard deviation of the timeseries. Drought conditions are indicated as SPI decreases below –1.0, while increasingly severe excess rainfall is indicated as SPI increases above 1.0.

Table 7. Drought classifications based on SPI.

Classification	SPI	Drought classes
1	SPI≥2.00	extreme wet
2	2.00>SPI≥1.50	very wet
3	1.50>SPI≥1.00	moderate wet
4	1.00>SPI≥-1.00	normal
5	-1.00≥SPI>-1.50	moderate drought
6	-1.50≥SPI>-2.00	severe drought
7	-2.00≥SPI	extreme drought

For data analysis and SPI calculation, the R programming language was used, through the software RStudio (Version 1.2.1335), along with the Standardised Precipitation Evapotranspiration Index "SPEI" package (Vicente-Serrano and Beguería 2010) which encompasses, a set of functions for computing potential evapotranspiration and several widely used drought indices including the SPI and SPEI. For the comparison of drought conditions among historical and future periods, histograms with dry and wet classes were drawn, based on the classification of SPI, as depicted in Table 7. Drought hazard has been analysed using SPI data output and frequency distribution diagrams in the R environment.

The following steps are presenting for the finalisation of drought hazard model:

a) Drought assessment for the entire period.

- Calculation of the mean monthly SPI6 as derived from the CMIP6 models for historical and future periods (under both SSPs) for the selected location.
- Classification of the index values based on Table 7 drought categories.
- Production of Frequency distribution diagrams.

Or

b) Drought assessment based on Dry (April to September) and Wet period (October to March), according to Hellenic National Meteorological Service (HNMS):

- Selection of SPI6 of March, as represented Index for Wet period.

ICARIA
Improving climate resilience
of critical assets

- Selection of SPI6 of September, as represented Index for Dry period.

- Calculation of the mean SPI6 as derived from the CMIP6 models for historical and future periods (under both SSPs) for the selected location.

- Classification of the drought values based on Table 7 drought categories.

- Production of Frequency distribution diagrams

4.3.3   Results of Test C

Drought hazard model is applied in a selected location in Rhodes Island, of the SAR region, as a case study of this methodology, examined in the framework of ICARIA.

The following figures 10, 11, and 12 show the classification of SPI6 which is changing under climate change scenarios, compared to the historical period by applying a+b methodologies. Consequently, the comparison between historical and future periods under different scenarios, is illustrated either by the use of methodology (a), that takes into consideration values of drought conditions for the entire year, or by applying methodology (b), which reflects the differences on drought conditions during dry and wet seasons of each year. The frequency of severe drought classes is projected to increase under ssp245. On the other hand, increased frequency is observed for moderate and severe wet conditions under ssp585.

Example 1: 3 CMIP6 MODELS RESULTS:
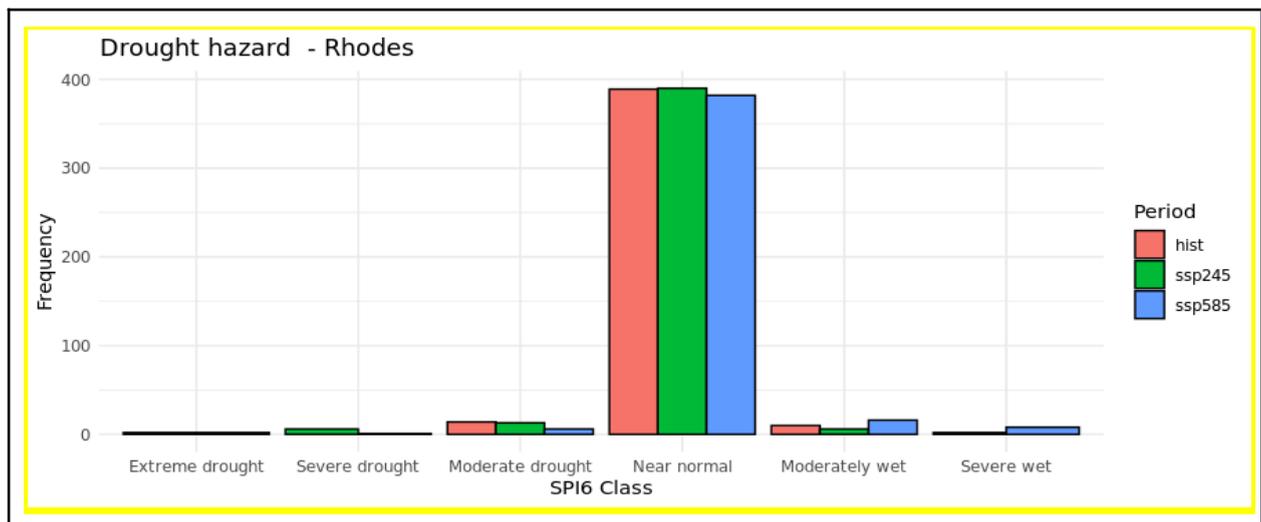
Figure 10. Example of SPI6 frequency distribution according to each drought class, for the historical (red color) and future period under ssp245 (green color) and ssp585 (blue color) for Rhodes.

Example 2: EC-EARTH3 MODEL RESULTS:
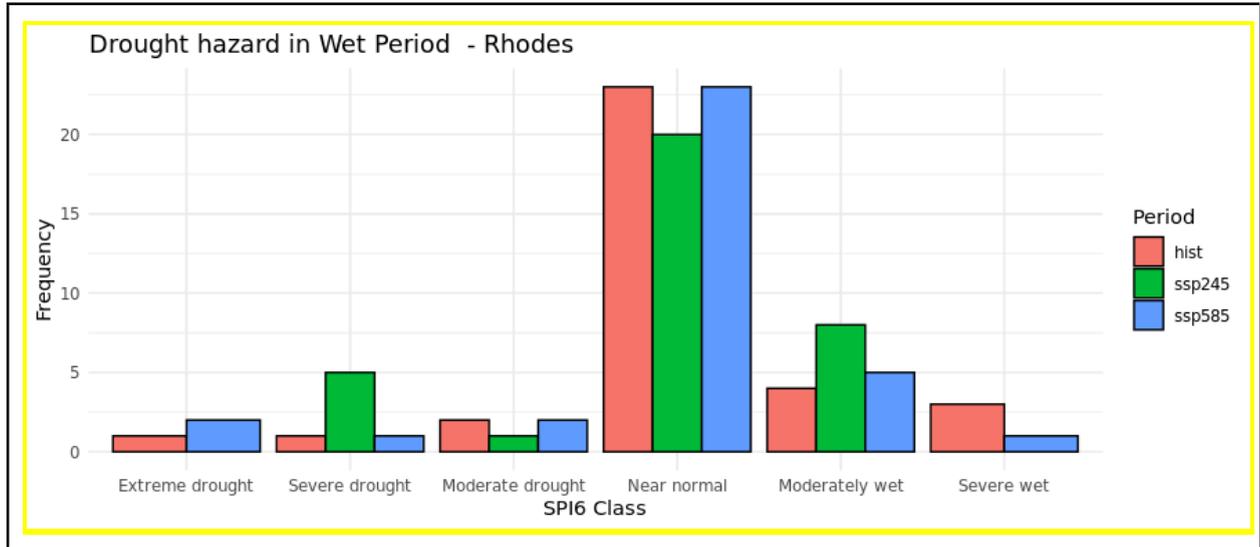
Figure 11. Example of SPI6 frequency distribution according to each drought class, for the **WET** historical (red color) and future period under ssp245 (green color) and ssp585 (blue color) for Rhodes.
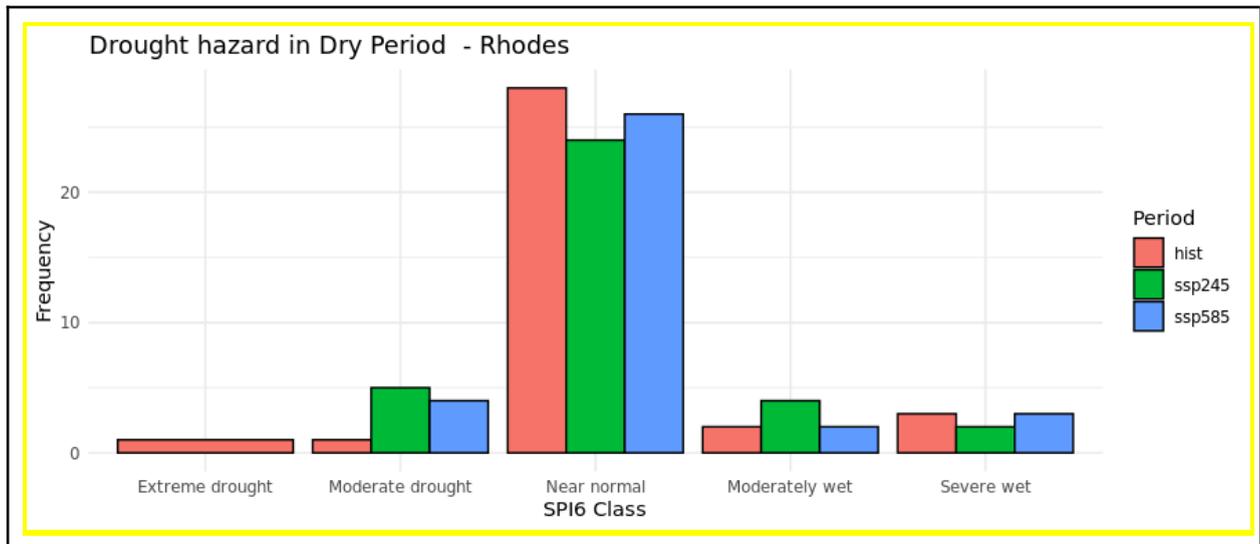
Figure 12 Example of SPI6 frequency distribution according to each drought class, for the **DRY** historical (red color) and future period under ssp245 (green color) and ssp585 (blue color) for Rhodes.

In general, based on the findings of the analysis, it is concluded that there are no detectable barriers or gaps present in the analysis. The above methodologies can be applied in both cases of statistical and dynamical downscaling. Therefore the drought hazard model analysis may illustrate drought conditions of a single point or for a total of gridded points (e.g. extended area), depending on the data availability and downscaling method, for the selected locations for each time period and climate

change scenario. The only limitation could be linked to the availability of the number of stations providing precipitation data that are considered for the generation of historical and future output of different CMIP6 models at the local scale, with the use of statistical downscaling methods.

4.4 Test D: Joint probability of occurrence of multi-hazard events

4.4.1 Summary and objectives of Test D

The objectives of this test are focused on the analysis of correlations within the climate data for selected compound hazard events across the three case studies to define the joint probability of these hazards either occurring simultaneously (compound coincident event) or sequentially (compound consecutive event) within a given timeframe.

Table 8. Test D summary.

Test D summary			
Tested tool	Python Code	**Test responsible**	UNEXE
Developer of the tool	UNEXE	**CS of the test**	AMB,SAR,SLZ

4.4.2 Activities of Test D

As part of the Joint Probability assessment for this deliverable one compound hazard type has been selected from each of the three case study regions as outlined in Table 9.

Table 9. Selected compound hazards for joint probability assessment.

Scenario number	Hazard 1	Hazard 2	Case Study Region
1	Pluvial Flooding	Storm Surge	AMB
2	Extreme Wind	Flooding	SLZ
3	Heatwave	Wildfire	SAR

Given that the respective climate datasets used to assess joint probability are at a daily resolution, the probability of Hazard 1 occurring simultaneously with, or within a specified timeframe of, Hazard 2 is also defined at a daily resolution, such that it defines the probability that an event will occur on a given day. As such, to approximate annual return periods (RPs), there is a need to convert from daily to annual probabilities. To do this, a simple mathematical approach has been employed, where once the initial probability is defined (*P(occuring in a day)*) the following 3 steps can be applied to convert to annual probabilities

1. Determine probability of event not occurring on a single day

$$P(not\ occuring\ in\ a\ day)\ =\ 1\ -\ P(occuring\ in\ a\ day)\quad (Eq.\ 5)$$

2. Probability of event not occurring on any day within a year

$$P(not\ occuring\ in\ a\ year)\ =\ P(not\ occurring\ in\ a\ day)^{365.25}\quad (Eq.\ 6)$$

where a year is assumed to be 365.25 days to factor in leap years into the calculation.

3. Probability of occurring at least once in a year

$$P(occurring\ at\ least\ once\ per\ year)\ =\ 1\ -\ P(not\ occuring\ in\ a\ year)\quad (Eq.\ 7)$$

Scenario 1: Pluvial Flooding and Storm Surge

For an initial assessment of Pluvial Flooding coinciding with Storm Surge events approximations of storm surge values vs daily cumulative rainfall is examined. For this test, a rain gauge has been selected near to the coastal area along with a corresponding Wave sensor buoy that is in proximity to the coast line and the rain gauge (Figure 13). For the climate analysis used within this assessment, a single climate model has been chosen, analysing historical data for the period of 1950 - 2014.
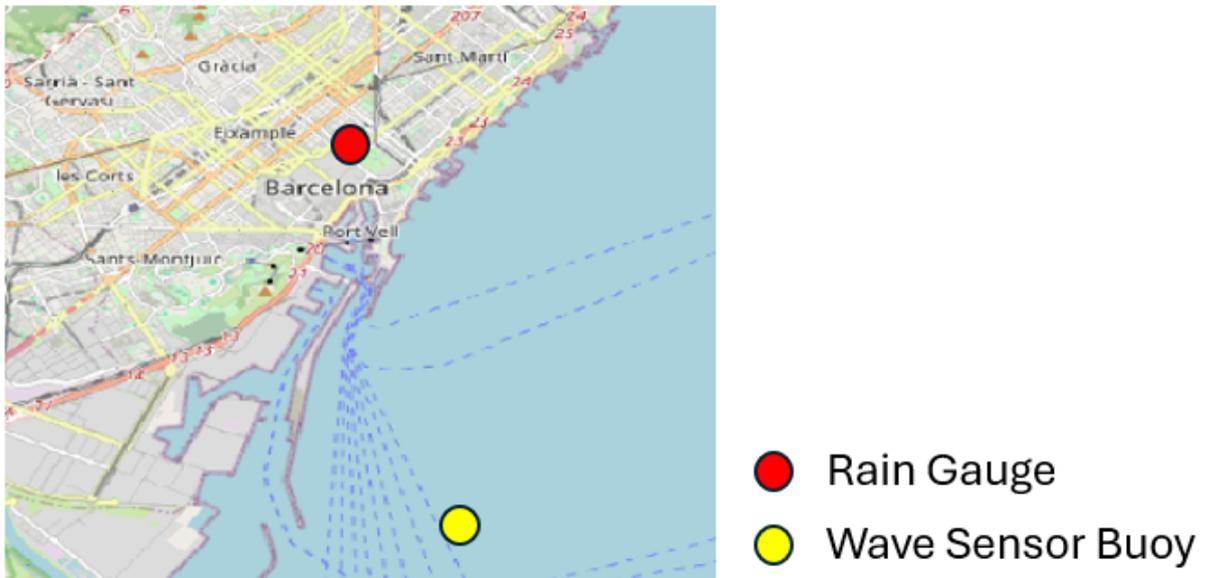
Figure 13. Location of rain gauge and sensor buoy for joint probability assessment.

With downscaled rainfall data being at daily resolution, the following definitions for significant rainfall events are being considered:

- Heavy precipitation day ≥ 20mm/day
- Severe heavy precipitation day ≥ 50mm/day
- Extreme precipitation day ≥ 100mm/day

To estimate Storm Surge (SS) values a combination of daily significant wave heights and tide data is derived with the following formula:

$$Storm\ Surge\ (SS)\ =\ Meteorological\ Tide\ (MT)\ +\ Wave\ Setup\ (S)\quad(Eq.\ 8)$$

where wave setup S is given by the approximation from Atkinson et al., (2017):

$$S{\sim}0.2H_s\quad(Eq.\ 9)$$

where:

- H_s is the offshore significant wave height

For extreme SS values in this analysis, the 90th percentile derived from annual maximums has been considered.

With both datasets being at daily resolution for defining compound events, the occurrence of significant rainfall events that take place within the region on the same day (overlapping time frames) of SS events that are equal to or exceed the 90th percentile value has been examined (Figure 14). In this example we can consider the magnitude of a storm surge event varying during the day along with the intensity and duration of the rainfall event, therefore from a physical modelling perspective these timeframes will need to be considered.
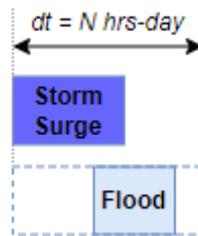
Figure 14. Depicting temporal range of compound Storm Surge and Flood Event.

Scenario 2: Extreme Wind and Flooding

For the modelling of the joint probability of extreme wind and flooding events, the analysis focuses on the probability of these events occurring either in the same region either simultaneously or sequentially within a specified number of days (N) following an extreme wind event (Figure 15).
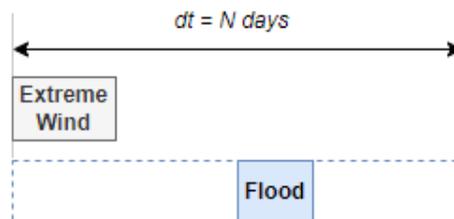
Figure 15. Depicting temporal ranges considered from compound wind and flood events.

Like that defined within scenario 1, the extreme rainfall events are classified in relation to their daily recorded values of 20mm/day, 50mm/day, and 100mm/day respectively. For the definition of extreme wind events, via discussion with stakeholders, a lower end wind gust speed relating to potential damage of trees has been selected with a value of 70 km/hr. As with scenario one, the time frame being analysed for this hazard combination is from 1950 - 2014.

With the implications of increased debris within the floodplain during and post event, this assessment will consider the probabilities of extreme rainfall coinciding with severe wind events and also occurring within a 30 day period of the extreme wind event.

Scenario 3: Heatwave and Wildfire

For this scenario, historical climate data was analysed from EC-EARTH3, models from 1980 to 2014.

The definition of a heatwave event for this test is defined the 95th percentile for summer months June, July, and August were used for during this period as the threshold temperature value whereby if said threshold is equal to or exceeded for 3 or more consecutive days then that period of time is considered to be a heatwave event (Figure 16).

Within Greece, fire weather season spans from May to October, as such the joint probability assessment carried out within this study will be focussed within these months. For defining a threshold of "fire danger" based on the Fire Weather Index (FWI) score one can consider either the extreme threshold (FWI >= 50) as defined by European Forest Fire Information System (EFFIS) using (Van Wagner et al., 1985) study, or the 90th percentile during the historical fire season. For analytical purposes in this assessment an FWI range of 20 (moderate) to 100 (extreme) is being considered.
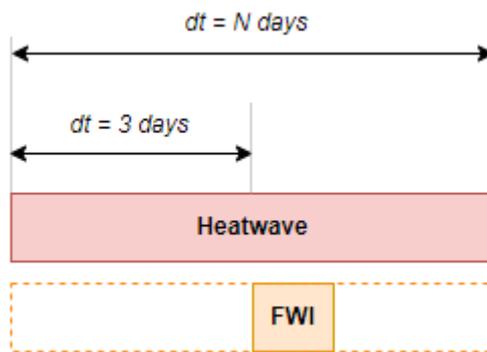
Figure 16. Depicting temporal ranges considered from compound Heatwave and FWI values.

4.4.3   Results of Test D

Summary of the main results of the test

Scenario 1: Pluvial Flooding and Storm Surge

Plotting daily rainfall values against maximum record wave height, it is possible to assess if there is correlation between the parameters. Figure 17 shows storm surge level estimate vs daily cumulative rainfall values and their corresponding marginal distributions. The marginal distributions highlight that the majority of days during this period experience no rainfall and that there is a lot of variation in wave heights on days where there is no rainfall occurring.
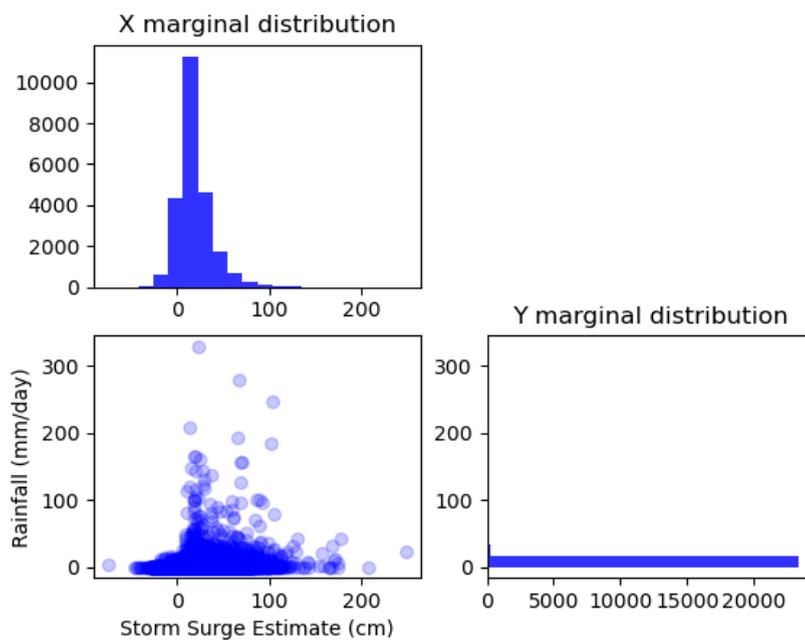
Figure 17. Analysis of Storm Surge level estimates Vs max daily rainfall.

To assess the joint probability for rainfall and and SS events, the exceedance probability for combinations of rainfall and SS values from the historical dataset should be estimated. Converting this dataset into a yearly joint probabilistic depiction (Figure 18) shows that heavy rainfall events (20mm/day) have an annual probability of occurrence close to 100% though the joint probability of such events occurring as storm surge levels increase the joint probability decreases. Analysing the joint probability an RP for specified extreme values of the historical data (Table 10) shows that the joint probability of SS and extreme rainfall events is not greater than the sum of their independent probabilities.
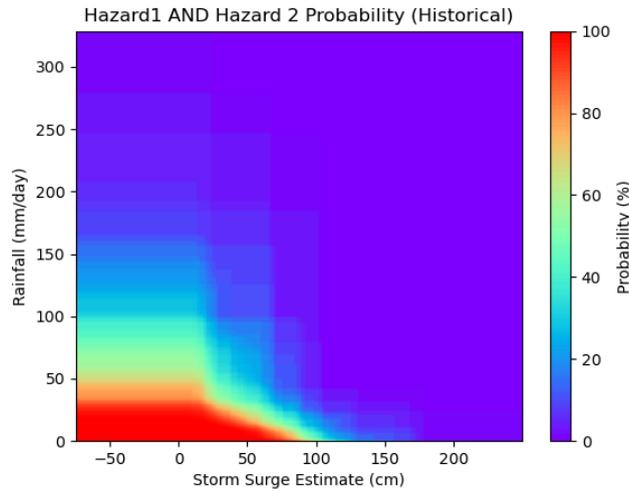
Figure 18. Annual probability of compound SS and Rainfall event.

Table 10. Joint probability summary of SS with Daily rainfall.

SS (cm)	Rainfall (mm/day)	Probability (%)	Return Period (Years)
-	20	98.44	1.02
-	50	65.99	1.52
-	100	31.94	3.13
44	-	100.00	1.00
44	20	75.03	1.33
44	50	28.73	3.48
44	100	10.21	9.79

Figures 17 and 18 showed significant variation in SS levels on days with low rainfall with extreme rainfall with Figure 17 also highlighting that heavier rainfall days tend to occur on days where storm surge estimates are on days where some inland surge occurs.

Scenario 2: Extreme Wind Vs Extreme Rainfall

Plotting wind speed Vs daily rainfall as shown in Figure 19 reveals that there is some correlation between wind speed and daily rainfall with higher recorded precipitation values observed during days where wind gust speeds are just below 50 km/hr.
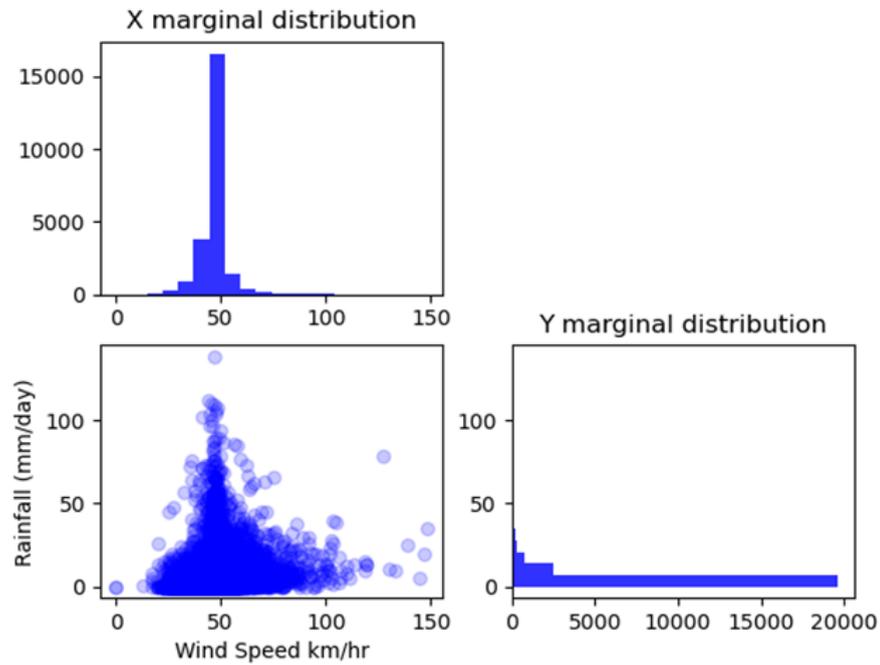
Figure 19. Analysis of wind speed Vs max daily rainfall.

Converting this data into its annual joint probability distribution (Figure 19) highlights the likelihood of extreme rainfall values coinciding with extreme wind events.
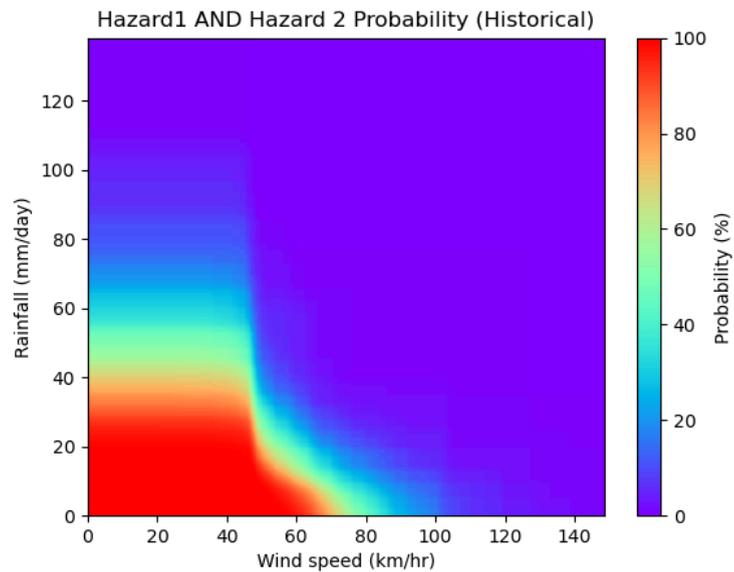
Figure 20. Annual joint probability of compound extreme wind and rainfall events.

For the statistical assessment of compound wind and rainfall hazard events, daily resolution wind gust data (km/day) and daily cumulative rainfall (mm/day) for a selected area in Salzburg were chosen. Through the analysis of this data, the probability of extreme events either occurring on the same day or the probability of extreme rainfall occurring within *N* days of an extreme wind event was assessed. Based on these daily probabilities their corresponding annual return periods were calculated. Table 11 summarises the derived return periods from assessing probability of occurrence for individual and compound coincident hazards at a daily resolution. Based on this historical analysis, it has been observed that whilst the minimum extreme thresholds are exceeded approximately annually, the coincidence of extreme wind and extreme rainfall occurs less frequently.

Table 11. Statistical analysis of compound coincident Wind Gust and Rainfall hazard from 1950 - 2014.

Wind Speed (km/hr)	Daily Rainfall (mm/day)	Probability (%)	Return Period (years)
70	-	98.75	1.01
-	20	100.0	1.0
70	20	45.99	2.17
-	50	87.35	1.14
70	50	4.51	22.17
-	100	14.26	7.0
70	100	0.0	No Occurrence

To assess the probability of extreme rainfall occurring within *N* days of an extreme wind event, iteration through the daily resolution wind gust data to identify days where wind gust speeds equal or exceed 70 km/hr has been performed. Using this date at a strat point, it is possible to iterate through the days to identify if and when threshold rainfall values are exceeded. Table 12 shows how the probability of extreme rainfall events occurring following a.n extreme rainfall event change over time. Here it is possible to observe that as the number of days increases the likelihood of an extreme rainfall event occurring does increase.

Table 12. Statistical analysis of compound consecutive Wind Gust and Extreme Rainfall from 1950 - 2014.

Wind Speed (km/hr)	Daily Rainfall (mm/day)	Day between events	Return Period (years)
70	20	5	1.46
70	20	10	1.21
70	20	20	1.10
70	20	30	1.06
70	50	5	11.33
70	50	10	9.79
70	50	20	7.73
70	50	30	6.42
70	100	5	65.5
70	100	10	65.5
70	100	20	33.0
70	100	30	33.0

Assessment of this historical data has highlighted that significant rainfall events tend to occur during days of relatively high wind gust speeds 50 km/hr and that significant rainfall events within 30 days of a severe wind storm event are likely to occur on an annual basis.

Scenario 3: Heatwave and Wildfire

To aid in visualising the potential relationship between heatwaves and FWI scores, the average 3 day (minimum duration of heatwave) temperature Vs FWI scores has been plotted for the island of Rhodes (Figure 21). Analysis of the FWI Vs temperature data shows an upward trend as average 3 day temperature increases. Within this dataset the 95th percentile for temperature value used in defining a heatwave was identified as being 32.8'C.

ICARIA
Improving climate resilience
of critical assets
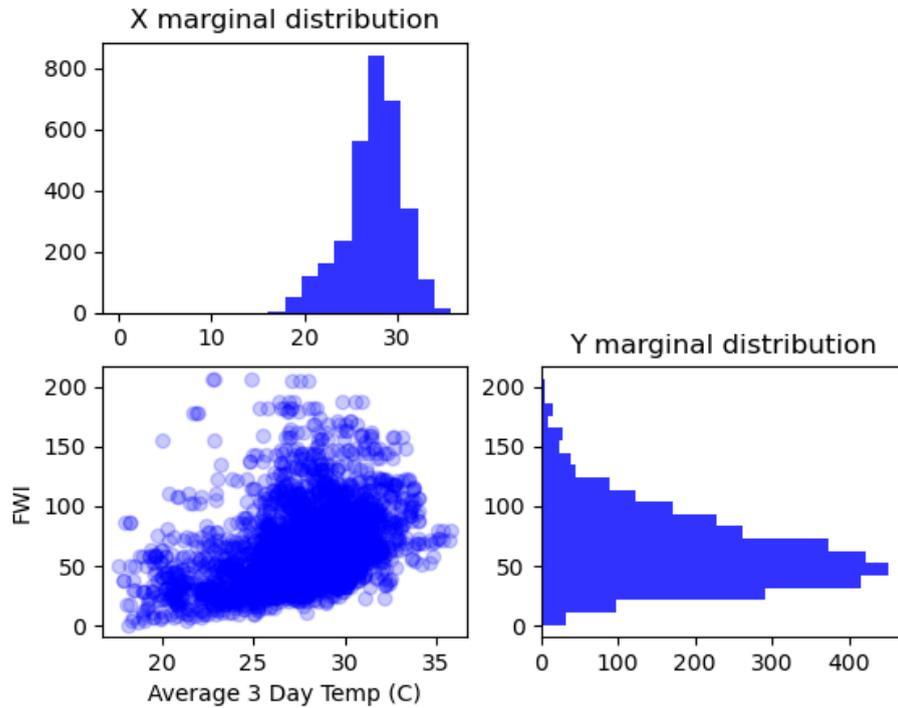
Figure 21. Example analysis of FWI scores Vs average 3 day temperature for Rhodes.

Through plotting the joint probability distribution of the average 3 day temperature Vs the FWI score we see that the annual probability of very extreme Fire Danger class (FWI >= 70) during the summer month is very high for a range of temperatures that are below the defined 32.8'C heatwave threshold criteria, with fire danger.
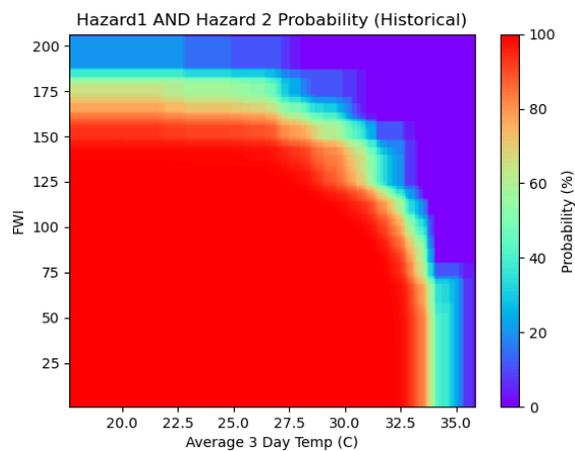
Figure 22. Annual joint probability of average 3 day temperature and FWI score.

Statistical analysis of the FWI score Vs the average 3 day temperature further highlights that extreme fire danger conditions within this region are likely an annual occurrence during the summer months.

Table 13. Statistical analysis of compound heatwave and FWI scores.

Heatwave 95th Percentile Temp (C)	FWI	Probability (%)	Return Period (years)
32.8	-	96.15	1.04
-	20	100.0	1.0
32.8	20	96.15	1.04
-	50	96.15	1.04
32.8	50	96.15	1.04
-	70	100.0	1.0
32.8	70	91.74	1.09
-	100	100.0	1.0
32.7	100	64.10	1.56

Based on the initial joint probability assessment of historical data from the Rhodes region we observe that there is a high likelihood of fire danger weather on an annual basis within the region that coincides with heatwave events however we also observe that heat waves themselves are not the primary driving factor in fire danger weather with high FWI scores featuring at lower temperature thresholds.

4.4.4   Summary of Test D

Visualising the joint probability distributions of compound hazard events highlights that for specified probabilities and respective return periods there exists a range of possible hazard combinations. For example, Figure 20 shows that for a compound extreme wind and rainfall event with a joint probability of 10% (1 in 10-year event) can be comprised of a range of values. This poses a challenge from the modelling perspective in terms of selection of input hazard parameters. Potential solutions for this could be the selection of respective median and 90th percentile values of the hazard values. Tables 14 and 15 show these values when considering wind speeds equal to or above the threshold 70 km/hr. Here we see that from the historical dataset we derive three unique compound hazard combinations that each correspond to a 1 in 10 year return period.

Table 14. Compound hazard combinations when deriving median and 90th percentile values from Wind speed

	Wind Speed (km/hr)	Rainfall (mm/day)
Median	109.25	13.14
90th Percentile	140.65	0.0

Table 15. Compound hazard combinations when deriving median and 90th percentile values from rainfall

	Wind Speed (km/hr)	Rainfall (mm/day)
Median	109.25	13.14
90th Percentile	76.26	29.88

An additional challenge in analysing such datasets relating to compound hazards, may relate to the rarity of such events when they are correlated within the tail end extremes. A couple of approaches for dealing with this limitation are the inclusion of more data from a range of climate models and SSPs to create a more robust climate dataset for analysis of joint probability and estimating uncertainty. A secondary approach would be to further analyse the dependencies between hazard drivers such as by the use of Copula as highlighted in Couasnon et al. (2018), whereby synthetic data can be generated via analysis of coupled datasets and their respective marginal distributions.

4.5 Test E: Heat wave hazard model on the electricity sector

4.5.1 Summary and objectives of Test E

The objective of test E has focused on analysing the effect of rising temperatures and heat waves and their interaction with the power grid model located in the AMB. The test refers to climate hazards on electrical grids and related impacts. For this reason, it can be considered a test that assesses both. Its objectives are to analyse how the data and information relevant to this study are received and processed, as well as how to process this information and match it with one of the critical infrastructures of the project.

This test has been selected because, in the AMB, similar studies have already been done with the flood hazards of the territory trial, such as in RESCCUE project (Russo et al., 2020)). In addition, among the AMB mini-trials, the one with the highest impact on the power grid is the heat wave.

The test aims to streamline two fundamental processes for future project packages: the first is the processing of climate data and the second is the design of the power grid model, which is the basis for seeing how the other hazards will impact the grid.

Table 16. Test E summary.

Test E summary			
Tested tool	QGIS and Python as tools for impact quantification	**Test responsible**	IREC, AQUA, AMB
Developer of the tool	IREC	**CS of the test**	AMB

4.5.2 Activities of Test E

The requirements for the assessment of hazard and impacts of a heat wave in the electrical sector of AMB are related to meteorological data and electrical grid data. The starting point of the meteorological data for the test is the historical data of the weather stations. These data consist of the periods of heat waves in the AMB and contain the location of the stations and the temperature measured every half an hour. From these data, temperatures are interpolated for each specific time and weather station to obtain a more extensive map of the heat wave.
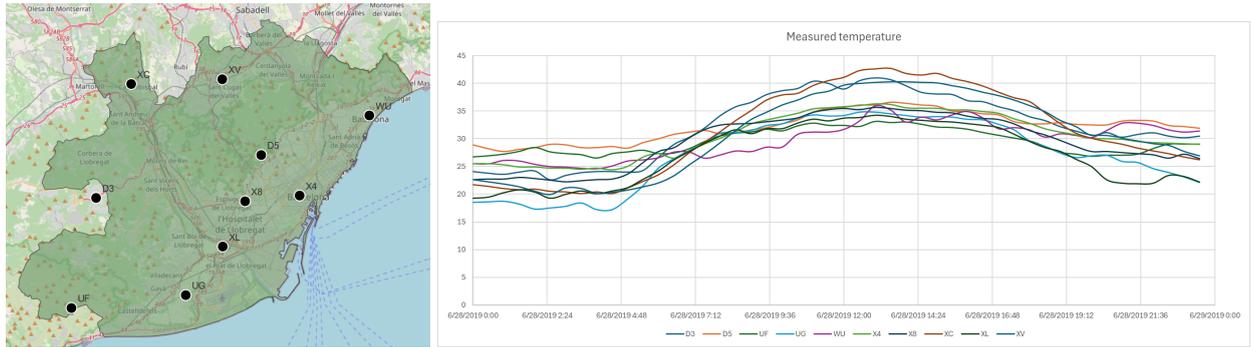
Figure 23. Meteorological stations with the heatwave data of the AMB region.

For the electricity grid model, the open data from the Open Street Maps platform is used. This data is subject to change in future project tasks when more detailed data is obtained from a local stakeholder. Furthermore, the electrical model is simplified by using only those elements directly affected by heat waves, such as overhead lines and electrical substations, as shown in Figure 24.
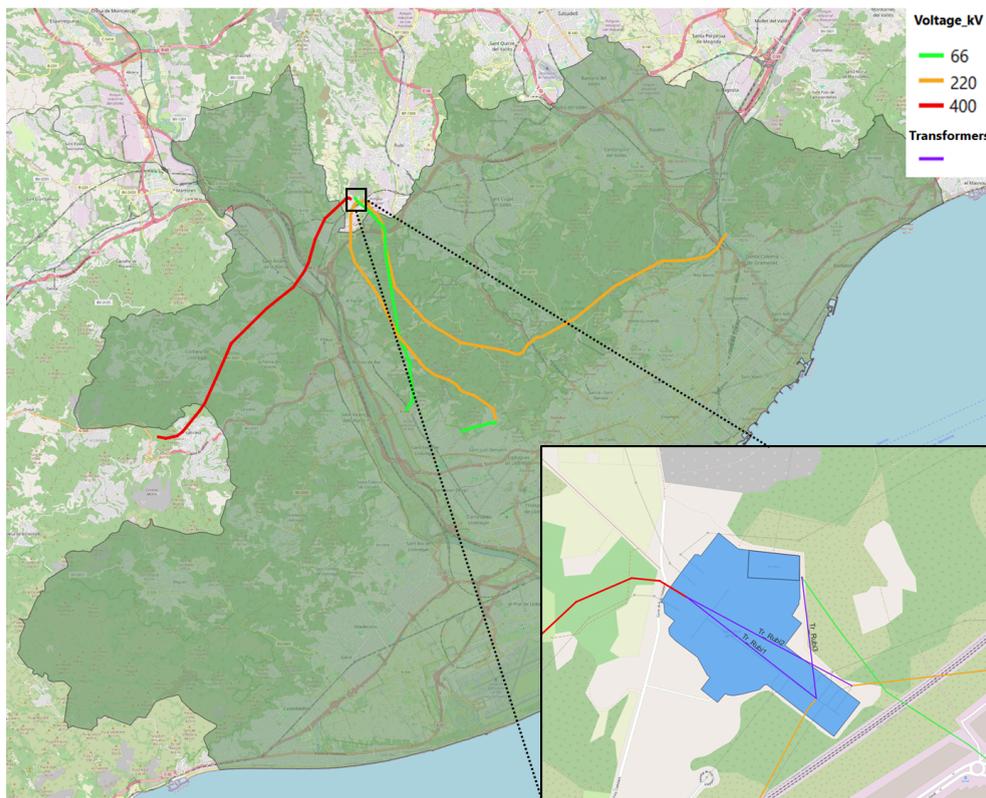
Figure 24. Georeferenced power grid with zoom to Rubi substation.

One reason why the model is simplified is that the data from the open source is not optimal for doing studies of power flow since the provided data is meant to give the georeferenced elements and their link with some relevant data, such as the voltage of the electric lines. In addition, the missing elements of the grid and the data's format make it incompatible with power flow programs. However, through the QGIS program and transforming the electrical network into the pandapower Python library (Thurner et al., 2018). Pandapower is an open-source code capable of power system modelling and analysis. It is composed of parametrized electric models of electrical elements, such as lines or transformers, that can be freely modified and customised. Furthermore, the power system analysis supports the power flow simulation. With these two aspects in mind, some crucial grid element models, such as the external electrical grid or the loads, have been added to the initial data, and it has been obtained a network with the necessary elements capable of making a power flow with and without taking into account the impacts of the heat wave as shown in Figure 25.
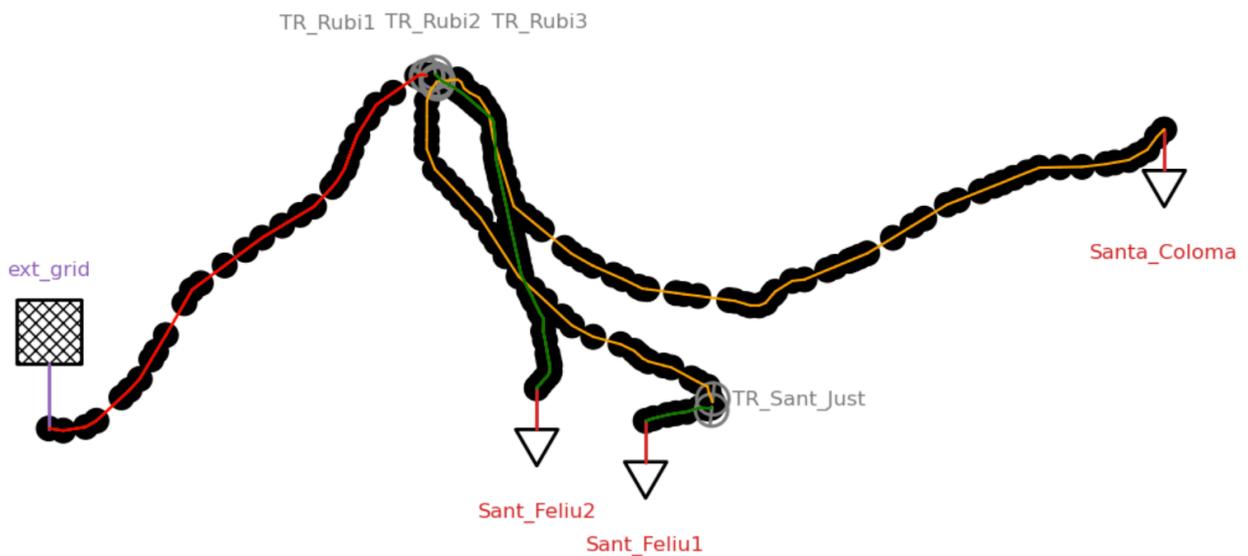
Figure 25. Pandapower model of the electrical network with its elements.

Once the power grid model and heatwave maps are ready, the information from both are cross-referenced to calculate the impacts of the hazard. It is done by assigning the temperature information of the heat wave to the electrical grid elements. In the case of the point elements (as it could be the consumption points), the temperature assigned is the one that overlaps with the model in the map. In contrast, in the case of lines, each line is assigned the average temperature that the line is stressed by. The equations defined and used for count the impact to the electric grid are the following ones collected in Deliverable 3.1 (Guerrero et al., 2024):

- Electricity demand: According to (Allen et al., 2016), the demand side of the power system changes due to two parameters during a heat wave event: the temperature and the latitude where the consumption is. In the formula, J represents the percentage increase in electricity demand, $L_{Centroid}$ denotes the latitude in decimal degrees at the territory's centroid, and ΔT stands for the change in maximum annual temperature. The equation that defines it, is the following one:

$$J = \left(9.594 - 0.1206 \cdot L_{Centroid}\right) \cdot \Delta T_C \quad (Eq.\ 10)$$

The total demand of the territory (D) is the calculation of the average customer demand (Davg) multiplied by the total number of customers (N) in it, and considering the percent increase of the demand due to the temperature rise and the latitude of the territory (J).

$$D = D_{av} \cdot N \cdot \left(1 + \frac{J}{100}\right) \quad (Eq.\ 11)$$

- Overhead lines: (Choobineh et al., 2016) approximated this equation for aluminium conductors steel reinforced (ACSR), which are most commonly used in overhead lines, and derived Eq.12. It represents how the power of the line decreases from 25ºC upwards.

$$\Delta P_{b,T}^{Line,max} = -0.768 \cdot T_t^a + 119.45 \quad (Eq.\ 12)$$

When subjected to an increase in electrical current, these lines may experience failures. (Lee et al., 2018) and (Bhatt et al., 2009) presented a fragility curve that relates how loaded the line is operating and the probability of that line failing; Figure 26 displays the results.
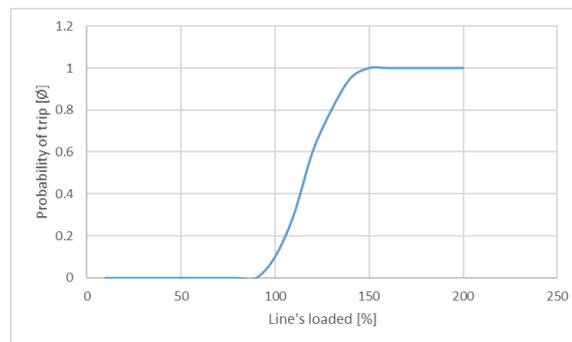
Figure 26. Fragility curve of how likely the line is to fail as a function of the load it supports.

- Substation power: for approximating the behaviour of the substation power, the results of (Hashmi et al., 2008) are taken as a reference. The study provides the relationship and how the capacity of the transformer varies by taking the ambient temperature as a reference.

$$\Delta P_T^{t\_power} = -0.0098 \cdot T_t^a + 1.1961 \quad (Eq.\ 13)$$

4.5.3 Results of Test E

To achieve results on the heat wave hazard and related impacts, the power grid is simulated with and without considering the ambient temperature of the elements. One of the assumptions is that the external energy arriving outside the AMB region is sufficient to supply the demand. A first simulation is done to take it as reference and to check the module works properly, as shown in Figure 27.

Figure 27. Power flow simulated without considering HW.

Once the first simulation with the nominal parameters of the grid is finished, a second simulation is done, taking into account the temperature they are stressed. Tables 17, 18, and 19 show how the capacity changes for the electrical elements in both simulations. It can be seen how the demand increases with more heat and conversely how the capacity of the electrical elements decreases with this increase. And Figure 28 shows the results of the simulation considering HW.

Table 17. Comparing the electricity demand and their change in both simulations.

Electricity demand	Active power	Temperature	New active power
[∅]	[MW]	[ºC]	[MW]
Sant Feliu de Guíxols	12.12	36.15	12.75
Sant Feliu de Guíxols 2	2.86	36.92	3.11
Santa Coloma de Gramenet	22.62	35.39	23.02

Table 18. Comparing six overhead lines of different voltages and stressed by different temperatures, their change in capacity for both simulations.

Lines	Maximum current	Temperature	New maximum current
[kV]	[kA]	[ºC]	[kA]
400	0.8067	41.08	0.71
400	0.8067	40.3	0.71
220	0.574	39.70	0.51
220	0.574	35.38	0.53
66	0.431	41.02	0.38
66	0.431	36.92	0.39

Table 19. Comparing the power substation and their change in both simulations.

Electricity demand	Capacity	Temperature	New Capacity
[∅]	[MVA]	[ºC]	[MVA]
TR_Rubi1	600	41.05	378.10
TR_Rubi2	600	41.05	378.10
TR_Rubi3	100	40.93	79.50
TR_Sant_Just	100	36.21	84.12

Figure 28. Power flow simulated considering HW.

The challenges faced along the test are related to the electricity model itself. The open data service has relevant information, such as the geographical location of some parts of the grid within their technical data. However, as mentioned before, it is not prepared for power flow simulation; this implies that it has to be transformed, and some assumptions have to be made. Even so, it has been enough to see how the heat wave map interacts with the model as well as to test the impact it would have on the electricity system.

Meanwhile, the interaction between meteorological data and the electricity model is straightforward since both are georeferenced. The transfer of information between them can be efficiently done with GIS software as it is QGIS.

4.6 Test F: Hazard assessment for Wildfire and Drought compound event to the SAR CS

4.6.1 Summary and objectives of Test F

The objective of Test F has been focused on a methodology that is based on the coincidence of dry conditions with extreme fire weather danger within a given timeframe, by investigating the statistics of corresponding indices that quantify each of the examined hazards for the SAR case study.

Regions prone to wildfire disasters, as SAR in the Mediterranean, are most likely to experience fire weather years preconditioned by drought (Richardson et al 2022). The prolonged low precipitation periods, commonly referred to as meteorological drought, increase the risk of forest fire events. Consequently, it is important to investigate the combination of dry conditions with high fire danger values.

Table 20. Test F summary.

Test F summary			
Tested tool	Compound hazards of Drought and Wildfire	**Test responsible**	DMKTS
Developer of the tool	DMKTS	**CS of the test**	SAR

4.6.2 Activities of Test F

For the conduction of trial Test F, it is primarily necessary the calculations of Standardised Precipitation Index (SPI) and Fire Weather Index (FWI) indices for the historical and future period for selected locations, based on daily precipitation, maximum temperature, relative humidity and wind gust datasets. These climate datasets were derived from the climate projections within ICARIA, by the application of statistical downscaling methodology (Blázquez et al., 2024). For the realisation of the trial, outputs for the Island of Rhodes were processed and can be, found here:

https://intercambio.ficlima.org/indexed/ICARIA/Climate_projections/SAR/

For this trial test, climate datasets from MRI-ESM2-0, MPI-ESM1-2-HR, and EC-EARTH3, CMIP6 models were analysed for the historical period (1980-2014) and for the future period up to 2050, under SSP245 and SSP585 scenarios.

    a) SPI6 calculation

The SPI is calculated by fitting a probability density function to a given frequency distribution of precipitation and then the probabilities are transformed into a normalised distribution with a mean

equal to zero and a variance of one, developed by Mckee et al. (1993). The distribution function used for computing SPI was the 'Gamma' as the most widely used in literature and recommended. Moreover, the SPI-6 was selected for drought hazard modelling, as in semi-arid and arid regions (as the study area), drought index computed at shorter accumulation periods could give unreliable estimates (Karavitis et al 2014). SPI calculated as follows in the equation:

$$SPI = \frac{X_I - X_J}{\sigma} \quad (Eq.\ 14)$$

where, x_i refers to the current precipitation in the examined period, x_j refers to the mean precipitation of the time series and σ refers to the standard deviation of the timeseries. Drought classification is provided in Table 21. Moreover, drought conditions are indicated as SPI decreases below −1.0, while increasingly severe excess rainfall is indicated as SPI increases above 1.0. To calculate the SPI, the R software was used, the "SPEI" package.

Table 21. Drought classifications based on SPI.

Classification	SPI	Drought classes
1	SPI≥2.00	extreme wet
2	2.00>SPI≥1.50	very wet
3	1.50>SPI≥1.00	moderate wet
4	1.00>SPI≥-1.00	normal
5	-1.00≥SPI>-1.50	moderate drought
6	-1.50≥SPI>-2.00	severe drought
7	-2.00≥SPI	extreme drought

b) FWI calculation

The Fire Weather Index (FWI) System is one of the two major subsystems of the Canadian Forest Fire Danger Rating System (CFFDRS). Their analytical presentation of the system equations and numerical codes describing the structure and components (see Figure 29) of the FWI System can be found in van Wagner and Pickett (1984). The higher the FWI is, the more favourable the meteorological conditions to trigger a wildfire. For each year, the fire season has length from May to October (officially in Greece) for FWI calculations. The calculation of the values of the Canadian FWI was performed using the package CFFDRS (https://r-forge.r-project.org/projects/cffdrs/) of R statistical computing software using as input four weather variables at 12:00 hours: temperature at 2m, relative humidity, wind speed at 10m, and daily precipitation.
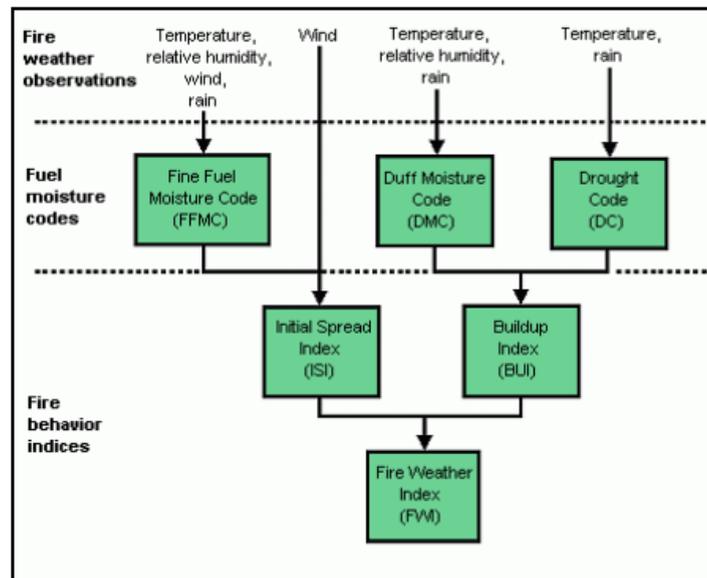
Figure 29. Structure of the FWI System
(https://cwfis.cfs.nrcan.gc.ca/background/summary/fwi).

The Fine Fuel Moisture Code (FFMC) is a numeric rating of the moisture content of litter and other cured fine fuels. This code is an indicator of the relative ease of ignition and the flammability of fine fuel. The Initial Spread Index (ISI) is a numeric rating of the expected rate of fire spread. It is based on wind speed and FFMC. Like the rest of the FWI system components, ISI does not take fuel type into account. Actual spread rates vary between fuel types at the same ISI.

Table 22. Fire Weather Classification classes according to EFFIS (source
https://forest-fire.emergency.copernicus.eu/about-effis/technical-background/fire-danger-forecast).

Fire Danger Classes	FWI	FFMC	ISI
Low	<11.2	< 86.1	< 5.0
Moderate	11.2 - 21.3	86.1 - 89.2	5.0 - 7.5
High	21.3 - 38.0	89.2 - 93.0	7.5 - 13.4
Very High	38.0 - 50	>=93.0	>=13.4
Extreme	50-70		
Very Extreme	>= 70		

c) Compound event during Fireseason

- Calculation of the monthly SPI6 as derived from the CMIP6 models for historical and future periods (for the selected SSPs) for the selected location.
- Calculation of the daily FWI as derived from the CMIP6 models for historical and future periods (for the selected SSPs) for the selected location.
- Common period for analysing the two indices: May to October

  o Extraction of SPI6 of October values, for each year, which represent the drought conditions of the entire fireseason.

  o Selection of drought years, based on the definition of drought conditions (-1.00≥SPI) of Table 22.

  o Statistical analysis and comparison of the extreme and mean values of the fire-related indices during these years in the historical (1980-2014) and future period (2015-2050) under SSPs:

    → Threshold of 90th percentile of FWI, ISI and FFMC
    → Number of very extreme fire days with FWI > 70.
    → Mean of FWI, FFMC and ISI

4.6.3 Results of Test F

Table 23 outlines the 90th percentile and the mean FWI values, along with the number of very extreme fire danger (FWI>70), according to EFFIS, only for the drought years and how these values are projected to change in the future under SSP245 and SSP585 in the island of Rhodes. Similar results are illustrated in Table 24 for the sub-components FFMC and ISI.

Example: 3 CMIP6 MODELS RESULTS:

Table 23. Drought and Wildfire: FWI statistical results derived from models for the historical period and the future under SSP245 and SSP585 for Rhodes, during drought years.

INDEX: FWI	FWI 90th Percentile	FWI mean	Number of days > 70
Historical	93.72	55.44	50.52
SSP245	91.72	58.26	52.72
SSP585	99.44	59.29	58.36

Table 24. Drought and Wildfire: ISI and FFMC statistical results derived from models for the historical period and the future under SSP245 and SSP585 for Rhodes, during drought years.

FFMC and ISI	ISI 90th Percentile	ISI mean	FFMC 90th Percentile	FFMC mean
Historical	42.81	21.52	90.77	87.57
SSP245	40.78	21.88	91.44	88.18
SSP585	46.60	23.51	91.23	88.04

Overall, the results indicated that during dry years, a moderate increase is observed in the statistics of the examined fire weather components under different SSPs, mainly under SSP585. In general, based on the findings of the analysis, it is concluded that there are no detectable barriers or gaps present in the analysis. Moreover, the above methodology can be applied in both cases of statistical and dynamical downscaling. Therefore the compound events hazard model analysis may illustrate the change signal based on the coincidence of dry conditions with extreme fire weather danger, within a given timeframe, for a single point or for a total of gridded points (e.g. extended area), depending on the data availability and downscaling method, for the selected locations. The only limitation could be linked to the availability of the number of stations providing wind speed/gust data considered for the application of statistical downscaling and therefore the generation of historical and future output timeseries of different CMIP6 models at the local scale for a single point/location, and in turn with the efficient calculation of FWI index and its subcomponents. Consequently, data provision imposes constraints on the assessment.

5 Conclusions

To conclude the task, the document aimed to validate different methodologies proposed in the framework of WP2. In order to accomplish this, six different tests have been performed for the three distinct regions of the project (AMB, SAR, and SLZ). These tests have been centred on analysing the dynamics and evaluating the consequences of climate hazards (tests A, B, C, and E). Furthermore, quantify the likelihood of compound hazard events, either coincident or consecutive (Tests D and F).

The first three tests, A, B, and C, have focused on the application of a single hazard model for a specific region. Each region has selected the hazard model considering their expertise and choosing one that has to be implemented in future project tasks, and at the same time, it has been tested very little, or never, in the region.

Thus, test A has consisted of the development of the Heat Island Hazard model for the AMB to analyse the effect of the increasing temperatures and heat waves. The test has obtained several results. The first one is the LST maps that help in the identification of the hot and cold spots of the region. The second one is the obtention of the vulnerability index and the selection of the critical areas distinguishing the census sections of the AMB. The last one is the result of a simplified part of the city map where, with the implementation of the SOLWEIG model, the test gets the Urban Heat Island temperatures. The test faced some barriers such as the need to evaluate night temperatures for UHI analysis and the limitation of using high-resolution nighttime images, leading to the use of Landsat daytime images for detailed urban impact assessment. Additionally, the search for disaggregated and up-to-date socioeconomic data for vulnerability analysis was challenging, with the most recent data being from 2021.

Test B has focused on the analysis of extreme wind hazard models for the SLZ region. The results conclude that the statistical reduction of wind gusts is handicapped by the scarcity of observational data, which leads to high uncertainty, especially in topographically complex areas such as Salzburg. Future models suggest weaker wind gusts, but their reliability is questionable. Dynamic downscaling also faces challenges due to errors in historical data and a lack of detailed wind information in the CHELSA dataset. Improvements are being sought through new post-processing methodologies and AI-based model weighting. The SLZ second CoP meeting highlighted the impact of wind speeds and directions on damage, highlighting the difficulty of accurately modelling local wind effects in complex terrain.

In the case of Test C, the hazard model implemented for the SAR region is the Drought Hazard model and has been applied to Rhodes Island. It evaluates the drought models CMIP6 and EC-EARTH3. The results obtained from the test are the frequency distribution of the drought classification periods (classified based on the SPI value) of the historical data and the future scenarios ssp245 and ssp585. Moreover, for the EC-EARTH3, the drought assessment has been divided into a dry period (April to September) and a Wet period (October to March) to get more detailed information. The outcomes show that under ssp245, severe drought classes are projected to increase the frequency of occurrence.

For Test D, all three CS have been considered. The test consists of correlation analysis within the climate data for selected compound hazard events to define the joint probability of these hazards, either simultaneously (compound coincident event) or sequentially (compound consecutive event) within a given time frame. Differently, from the first three tests, the hazards selected to conduct Test D have no restriction, even though they have been studied individually on other projects since no previous studies

were done, considering them happening simultaneously or sequentially. Therefore, in the AMB scenario, the hazards considered have been pluvial flooding and storm surges. In the SLZ scenario, it treated extreme wind and flooding, and in the SAR scenario, the hazards considered are heatwave and wildfire.

The results in Test D show the correlation between the main variables of the hazards under study for the three scenarios. In the AMB and SLZ cases, it is presented the return period of the two risks for each scenario to happen coincidentally. Moreover, for the SLZ case, it calculates with the use of the historical data the likelihood of having the extreme wind and flooding consecutively, giving the return period of having both hazards successive, considering the days between both events. For the SAR case, the initial joint probability assessment of historical data from the Rhodes region indicates a high likelihood of fire danger weather on an annual basis coinciding with heatwave events. However, it also reveals that heat waves are not the primary driving factor in fire-danger weather, as high FWI scores occur at lower temperature thresholds.

Test E has focused on the crossing of heat wave hazards with one of the assets of interest in the project, which is the electrical grid. The results show that the combination of meteorological data with power grid model data is a relatively straightforward process with the use of GIS software due to both being geo-referenced. Furthermore, it has served as a test for hazard and impact assessment.

Test F has developed and analysed the compound wildfire and drought hazard to the SAR CS, specifically on Rhodes Island. The methodology is based on the coincidence of drought conditions with the extreme meteorological danger of fire at a given time. The results show the 90th percentile and the mean FWI, FFMC, and ISI values, along with the number of very extreme fire danger (FWI>70), only for the drought years and how these values are projected to change in the future under SSP245 and SSP585.

Overall, through the tests performed in the deliverable, it has been possible to validate most of the methodologies proposed in Work Package 2 in certain regions with little experience with them, along with their connection with the other work packages. In addition, these tests have helped identify possible barriers to be encountered in the following tasks and provided a basis from which to proceed.

6 References

Allen, M. R., Fernandez, S. J., Fu, J. S., & Olama, M. M. (2016). Impacts of climate change on sub-regional electricity demand and distribution in the southern United States. Nature Energy, 1(8), 1-9.

Ajuntament de Barcelona (9th july , 2019) Red de refugios climáticos. Barcelona por el Clima, Urbanismo, Transición Ecológica, Servicios Urbanos y Vivienda. https://www.barcelona.cat/barcelona-pel-clima/es/acciones-concretas/red-de-refugios-climaticos.

Atkinson, A.L., Power, H.E., Moura, T., Hammond, T., Callaghan, D.P., Baldock, T.E., 2017. Assessment of runup predictions by empirical models on non-truncated beaches on the south-east Australian coast. Coast. Eng. 119, 15–31. https://doi.org/10.1016/j.coastaleng.2016.10.001.

Bhatt, N., Sarawgi, S., O'keefe, R., Duggan, P., Koenig, M., Leschuk, M., … & Povolotskiy, M. (2009). Assessing vulnerability to cascading outages. In 2009 IEEE/PES Power Systems Conference and Exposition (pp. 1-9). IEEE.

Blázquez C. et al (2024). ICARIA Climate projections and hazard scenarios. ICARIA, Deliverable 1.2, H2020 grant no. 101093806, Sections 2.1 and 3.2.

Cheikh Faye, Manuela Grippa, Stephen Wood. Use of the Standardized Precipitation and Evapotranspiration Index (SPEI) from 1950 to 2018 to determine drought trends in the Senegalese territory. Climate Change, 2019, 5(20), 327-341.

Choobineh, M., Tabares-Velasco, P. C., & Mohagheghi, S. (2016). Optimal energy management of a distribution network during the course of a heat wave. Electric Power Systems Research, 130, 230-240.

Couasnon, A.; Sebastian, A.; Morales-Nápoles, O. A Copula-Based Bayesian Network for Modeling Compound Flood Hazard from Riverine and Coastal Interactions at the Catchment Scale: An Application to the Houston Ship Channel, Texas. Water 2018, 10, 1190. https://doi.org/10.3390/w10091190.

Febrian, A. & Darmawan, Y. (2024). Spatial–Temporal Analysis of Urban Heat Island (UHI) in Bandung Raya Using Remote Sensing Data. DOI 10.1007/978-981-97-0740-9.

Guerrero, M., de la Cruz Coronas, A., Flor, G., Evans, B., Gili, A. (2024). Tangible Impact Assessment Methods. ICARIA Project Deliverable D3.1. 136 pp.

Haiden, T., Kann, A., Wittmann, C., Pistotnik, G., Bica, B., & Gruber, C. (2011). The Integrated Nowcasting through Comprehensive Analysis (INCA) system and its validation over the Eastern Alpine region. Weather and Forecasting, 26(2), 166-183.

Halder, B., Karimi, A., Mohammad, P., Bandyopadhyay, J., Brown, R. & Yaseen, Z. (2022). Investigating the relationship between land alteration and the urban heat island of Seville city using multi-temporal Landsat data. Theoretical and Applied Climatology. DOI 150. 10.1007/s00704-022-04180-8.

Hashmi, G. M., Lehtonen, M., & Millar, R. J. (2008). Transformer Loading Conditions for Future Thermally Unfavourable Environments. In International Conference on Electrical and Control Technologies, ECT08, Kaunas, Lithuania, May 8-9, 2008.

He, B.J., Wang, J., Liu, H. & Ulpiani, G. (2020). Localized synergies between heat waves and urban heat islands: Implications on human thermal comfort and urban heat management. Environmental Research. 193. DOI 110584. 10.1016/j.envres.2020.110584.

Hidalgo, D. (2021). Analysis and precision of the Terrestrial Surface Temperature using Landsat 8 and Sentinel 3 images: Study applied to the city of Granada (Spain). Sustainable Cities and Society. 71. 102980. DOI 10.1016/j.scs.2021.102980.

Höppe, P. (1992). A new procedure to determine the mean radiant temperature outdoors. Wetter unt Leben, 44, 147-51.

Karavitis, C.A.; Tsesmelis, D.E.; Skondras, N.A.; Stamatakos, D.; Alexandris, S.; Fassouli, V.; Vasilakou, C.G.; Oikonomou, P.D.; Gregorič, G.; Grigg, N.S.; et al. Linking Drought Characteristics to Impacts on a Spatial and Temporal Scale. Water Policy 2014, 16, 1172–1197, doi:10.2166/wp.2014.205.

Karger, D. N., Lange, S., Hari, C., Reyer, C. P., Conrad, O., Zimmermann, N. E., & Frieler, K. (2022). CHELSA-W5E5: Daily 1 km meteorological forcing data for climate impact studies. Earth System Science Data Discussions, 2022, 1-28.

Karger, D. N., Conrad, O., Böhner, J., Kawohl, T., Kreft, H., Soria-Auza, R. W., … & Kessler, M. (2017). Climatologies at high resolution for the earth's land surface areas. Scientific data, 4(1), 1-20.

Lee, S. T. (2008). Estimating the probability of cascading outages in a power grid. Proc. of 16th PSCC, Glasgow, Scotland, 14-18.

Lindberg, F., Holmer, B., & Thorsson, S. (2008). SOLWEIG 1.0—Modelling spatial variations of 3D radiant fluxes and mean radiant temperature in complex urban settings. International journal of biometeorology, 52, 697-713. DOI 10.1007/s00484-008-0162-7.

Mckee, T.B.; Doesken, N.J.; Kleist, J. The Relationship of Drought Frequency and Duration to Time Scale. In Proceedings of the Eighth Conference on Applied Climatology; 1993; pp. 17–22.

Ministerio de Transportes, Movilidad y Agenda Urbana, (7th march, 2023). Urban3r. Plataforma de Datos Abiertos para impulsar la regeneración urbana en España. https://datos.gob.es/es/aplicaciones/urban3r

Possega, M., Aragão, L., Ruggieri, P., Santo, M. & Di Sabatino, S. (2022). Observational evidence of intensified nocturnal urban heat island during heat waves in European cities. Environmental Research Letters. 17. DOI 10.1088/1748-9326/aca3ba.

Rees, G., Hebryn-Baidy, L. & Belenok, V. (2024). Temporal Variations in Land Surface Temperature within an Urban Ecosystem: A Comprehensive Assessment of Land Use and Land Cover Change in Kharkiv, Ukraine. Remote Sensing. 16. 1637. DOI 10.3390/rs16091637.

Renard, F., Lucille, A., Fitts, Y., Hadjiosif, A., & Comby, J. (2019). Evaluation of the Effect of Urban Redevelopment on Surface Urban Heat Islands. Remote Sensing. 11. 299. DOI: 10.3390/rs11030299.

Richardson, D., Black, A.S., Irving, D. et al. Global increase in wildfire potential from compound fire weather and drought. npj Clim Atmos Sci 5, 23 (2022). https://doi.org/10.1038/s41612-022-00248-4.

Russo, B.; Velasco, M.; Locatelli, L.; Sunyer, D.; Yubero, D.; Monjo, R.; Martínez-Gomariz, E.; Forero-Ortiz, E.; Sánchez-Muñoz, D.; Evans, B.; et al. Assessment of Urban Flood Resilience in Barcelona for Current and Future Scenarios. The RESCCUE Project. Sustainability 2020, 12, 5638, https://doi.org/10.3390/su12145638.

Stucki, P., Dierer, S., Welker, C., Gómez-Navarro, J. J., Raible, C. C., Martius, O., & Brönnimann, S. (2016). Evaluation of downscaled wind speeds and parameterised gusts for recent and historical windstorms in Switzerland. Tellus A: Dynamic Meteorology and Oceanography, 68(1), 31820.

Thurner, L., Scheidler, A., Schäfer, F., et al, (2018). pandapower - an Open Source Python Tool for Convenient Modeling, Analysis and Optimization of Electric Power Systems, in IEEE Transactions on Power Systems, vol. 33, no. 6, pp. 6510-6521.

Waleed, M. & Sajjad, M. (2021). Leveraging cloud-based computing and spatial modeling approaches for land surface temperature disparities in response to land cover change: Evidence from Pakistan. Remote Sensing Applications: Society and Environment. 25. DOI:10.1016/j.rsase.2021.100665.

Ward, K., Lauf, S., Kleinschmit, B. & Endlicher, W. (2016). Heat waves and urban heat islands in Europe: A review of relevant drivers. Science of The Total Environment. 569-570, 527–539. DOI 10.1016/j.scitotenv.2016.06.119.

Van Wagner, C.E.; Pickett, T.L. Equations and FORTRAN Program for the Canadian Forest Fire Weather Index System; 1985.

S.M. Vicente-Serrano, S. Beguería, J.I. López-Moreno. 2010. A Multi-scalar drought index sensitive to global warming: The Standardized Precipitation Evapotranspiration Index – SPEI. Journal of Climate 23: 1696, DOI: 10.1175/2009JCLI2909.1.

Yuan, Y., Dong, X., Chengwei, L., Xiaolei G., Zhou, Y., Fan, Z., Liao, C. & Wang, X. (2023). The Growing Threat of Global Urban Heat Island Effects in Lower-Middle- and Low-Income Countries. 10.21203/rs.3.rs-2922430/v1.

Zhao, L., Oppenheimer, M., Zhu, Q., Baldwin, J., Ebi, K., Bou-Zeid, E., Guan, K. & Liu, X. (2018). Interactions between urban heat islands and heat waves. Environmental Research Letters. 13. DOI 10.1088/1748-9326/aa9f73.

Annex A: Data Management Statement

Table A.1. Data used in preparation of ICARIA Deliverable 2.5.

Dataset name	Format	Size	Owner and re-use conditions	Potential utility within and outside ICARIA	Unique ID
na	na	na	na	na	na

Table A.2. Data produced in preparation of ICARIA Deliverable 2.5.

Dataset name	Format	Size	Owner and re-use conditions	Potential utility within and outside ICARIA	Unique ID
na	na	na	na	na	na

More info: **www.icaria-project.eu**